Annual to Interannual Equatorial Atlantic Variability: Mechanisms and Tropical Impacts

Dissertation
zur Erlangung des Doktorgrades
der Mathematisch Naturwissenschaftlichen Fakultät
der Christian-Albrechts-Universität zu Kiel
vorgelegt von

Hui Ding

Department of Meteorology,
Research Division of Ocean Circulation and Climate Dynamics
Leibniz Institute of Marine Sciences
Kiel University, Kiel, Germany

June 2010

Referent: Prof. Dr. Mojib Latif
Koreferent: Dr. Noel Keenlyside
Tag der mndlichen Prfung: 19.07.2010
Zum Druck genehmigt: 19.07.2010
gez. Prof. Dr. Lutz Kipp, Dekan

Contents

Abstract

In this thesis, I investigate the annual to interannual variability in the equatorial Atlantic and its impacts on other tropical oceans. There are three parts to this work. The first part (chapter 2) is to understand the seasonal cycle of ocean dynamics, which has been published in 2009. The second part (chapter 3) is to understand the mechanisms of interannual variability in the equatorial Atlantic, which is mainly associated with Atlantic zonal mode. This part has been accepted recently for publication and is in press. The last part (chapter 4) investigates the influence of Atlantic zonal mode on El Niño Southern Oscillation in a coupled climate model. This work will be submitted for publication.

In chapter 2, the dynamics of the seasonal cycle in the upper equatorial Atlantic ocean are studied using observations and a hierarchy of ocean models. Distinctive features of the seasonal cycle are strong annual and semi-annual components; eastward (westward) propagating sea surface height (SSH) and thermocline depth at the equator (off the equator); and westward propagating surface zonal currents at the equator. Modelling results show that linear theory can explain the seasonal cycle in thermocline depth and SSH. While to first order linear theory can also explain the structure of the seasonal cycle of surface zonal currents at the equator, nonlinear terms are required. The linear solution is essentially determined by the four gravest baroclinic modes, and Kelvin and first meridional mode Rossby waves. The semi-annual cycle in zonal winds although much weaker than the annual component forces a strong semi-annual component in SSH and surface zonal currents, because it excites the basin mode of the second baroclinc mode.

The second part of the thesis investigates the dynamics of the Atlantic zonal mode using observed sea surface height (SSH), sea surface temperature (SST), and heat flux and reanalysis wind stress and upper ocean temperature. Principal oscillation pattern (POP) analysis shows that the zonal mode is an oscillatory normal-

mode of the observed coupled system, obeying the delayed-action/recharge oscillator paradigm for ENSO. Net surface heat flux anomalies generally act to damp SST anomalies. The zonal mode explains a large amount (70%) of SST variability in the east and a significant fraction (19%) of equatorial variability. Thus, the predictability potential in the Equatorial Atlantic on seasonal time scales may be considerably higher than currently thought.

In the third part, a coupled climate model is employed to investigate the influence of Atlantic zonal mode on ENSO in the Pacific. Five ensemble member simulations forced with observed sea surface temperature in the Tropical Atlantic, but with full air-sea coupling allowed elsewhere, were performed for the period 1950-2005. Model results show that a warm phase of Atlantic zonal mode during boreal summer favours the development of a La Niña event during the boreal winter and vice versa. A warm SST anomaly in the Atlantic affects the Walker Circulation with anomalous rising and subsiding motions in the Tropical Atlantic and eastern Tropical Pacific, respectively. This causes an easterly anomaly to the west of subsiding region in the Pacific that is amplified by the Bjerknes positive feedback, favouring the following development of a La Niña event. In general, the coupled model has revealed the same mechanisms of how Atlantic zonal mode influence ENSO as found in observations and reanalysis. This is the first convincing evidence from a model for the existence of a physically robust influence of the Atlantic Zonal mode on Pacific interannual variability.

Zusammenfassung

Gegenstand dieser Arbeit ist die saisonale bis mehrjährige Variabilität des äquatorialen Atlantiks und deren Auswirkung auf die anderen tropischen Ozeane. Die Arbeit besteht aus drei Teilen. Der erste Teil (Kapitel 2) dient dem Verständnis des Jahresgangs der dynamischen Prozesse im Ozean (2009 veröffentlicht). Im zweiten Teil werden die Mechanismen zwischenjährlicher Variabilität im äquatorialen Atlantik untersucht, die vor allem den sogenannten Atlantic Zonal Mode betreffen. Der Publikation dieses Abschnitts wurde gerade zugestimmt; der Artikel erscheint in den kommenden Wochen. Der letzte Teil der Arbeit (Kapitel 4) zeigt den Einfluss des Atlantic Zonal Modes auf ENSO (El Niño Southern Oscillation) in einem gekoppelten Klimamodell. Diese Arbeit wird in Kürze zur Veröffentlichung eingereicht.

Im ersten Teil der Arbeit werden auf Grundlage von Beobachtungen und Ozeanmodellen unterschiedlicher Komplexität die Dynamik des Jahresgangs im oberen äquatorialen Atlantischen Ozean untersucht. Besonders ausgeprägt sind jährliche und halbjährliche Fluktuationen im jahreszeitlichen Zyklus; zum einen die ostwärts (bzw. westwärts) gerichtete Ausbreitung der Meeresspiegelhöhe SSH (Sea Surface Height) sowie die Tiefe der Thermokline am Äquator (bzw. neben dem Äquator) und zum anderen die nach Westen gerichtete zonale Oberflächenströmung am Äquator. Die Modellergebnisse bestätigen, dass man den saisonalen Zyklus von Thermoklinen-Tiefe und SSH mittels linearer Theorie erklären kann. Ebenso kann die Struktur der jahreszeitlichen Variabilität der Oberflächenströmung am Äquator mittels linearer Theorie abgeschätzt werden; zu deren genauerer Bestimmung sind zusätzliche nichtlineare Therme nötig. Die lineare Lösung wird maßgeblich durch die vier Modes der Baroklinität im Ozean, sowie der Kelvin-Welle und den ersten meridionalen Mode der Rossby-Wellen bestimmt. Der halbjährliche Zyklus zonaler Winde verstärkt die (ebenso halbjährlichen) Komponenten von SSH und zonaler Oberflächenströmung mehr als der eigentlich stärker ausgeprägte ganzjährliche Zyklus, denn er vergrößert

den Einfluss des zweiten baroklinen Modes.

Der zweite Teil beschäftigt sich mit der Dynamik des Atlantic Zonal Modes unter Berücksichtigung von Beobachtungsdaten der Wasseroberflächenhöhe (SSH), der Oberflächentemperatur (SST Sea Surface Temperature) und des Wärmeflusses, sowie Re-Analyse Daten des Wind-Stresses und des Temperaturprofils im oberen Ozean. Die Analyse der Principle Oscillation Patterns POPs zeigt, dass der zonale Modus einer Normalschwingung des beobachteten gekoppelten Systems entspricht, wenn man die gängigen ENSO-Theorien zugrunde legt (recharge oscillator paradigm for ENSO). Die Gesamt-Anomalien des Oberflächen-Wärmeflusses dämpfen im Allgemeinen die SST-Anomalien. Der zonale Modus erklärt einen Großteil der SST-Variabilität im Osten (70 %) und einen signifikanten Anteil an äquatorialer Variabilität (19 %). Das Potential für die Vorhersagbarkeit des Zustands des äquatorialen Atlantiks muss damit viel höher bewertet werden als bisher angenommen.

Im letzten Abschnitt wird ein gekoppeltes Klimamodell eingesetzt, um den Einfluss des Atlantic Zonal Modes auf ENSO im Pazifik zu untersuchen. Dazu werden fünf Modell-Konfigurationen für den Zeitraum 1950-2005 miteinander verglichen. Beobachtungsdaten der Oberflächentemperatur im tropischen Atlantik dienen als Antrieb in den Simulationen; außerhalb des tropischen Atlantiks ist eine vollständige Atmosphären-Ozean-Kopplung gegeben. Die Simulationsergebnisse belegen eine Begünstigung der Entwicklung von La Niña Ereignissen während des borealen Winters aufgrund einer Warmphase des Atlantic Zonal Modes im borealen Sommer und umgekehrt. Eine warme SST-Anomalie im Atlantik beeinflusst die Walker-Zirkulation mit entsprechend anomalen aufwärts- und abwärts Bewegungen im tropischen Atlantik bzw. im östlichen tropischen Pazifik. Das verursacht eine Wind-Anomalie (easterly anomaly) im westlichen Pazifik, die durch das Bjerknes Positiv-Feedback verstärkt wird und die Entwicklung des kommenden La Niña Ereignisses begünstigt. Das gekoppelte Modell zeigt prinzipiell die gleichen Mechanismen einer

ENSO-Beeinflussung durch Atlantik Niño, wie sie bei Beobachtungen und Re-Analyse-Daten gefunden wurden. Damit ist der erste überzeugende Beweis für die Existenz eines Einflusses des Atlantic Zonal Modes auf die zwischenjährliche Variabilität im Pazifikerbracht worden.

Chapter 1

Introduction

The Tropical Atlantic Ocean is flanked by two large tropical continents, which host major centers of atmospheric convection. About three centuries ago, Halley [1686] recognized the important influence of these continents on climate in the Atlantic Ocean. Since 1970s, the influence of the Tropical Atlantic Ocean on continental climate variability began to come to light [*Xie and Carton*, 2004], as it was realised that it hosts pronounced variability on annual to interannual timescales. The seasonal cycle in Atlantic Ocean interacts with and regulates the meridional excursions of the Atlantic intertropical convergence zone (ITCZ), and so rainfall over surrounding countries. Numerous studies have shown that interannual variability in rainfall over the South America and West Africa is associated with well-organized, repeating patterns of sea surface temperature (SST) and Trade Wind anomalies over the Tropical Atlantic Ocean [*Xie and Carton*, 2004]. As will be discussed, while both annual and interannual variability in the Tropical Atlantic exhibit similarity to that in the Tropical Pacific, key differences exist that remain to be fully understood. Therefore, it is of scientific and socio-economic interests to study Tropical Atlantic variability.

Sea surface temperature (SST) displays a pronounced annual cycle at the equator although the Sun crosses the equator twice per year [*Mitchell and Wallace*, 1992; *Xie*

and Carton, 2004]. The annual cycle in the Tropical Atlantic displays very similar evolution to that in the Tropical Pacific in atmospheric circulation and sea surface temperature [*Mitchell and Wallace*, 1992]. This is probably why previous studies [*Chang and Philander*, 1994; *Xie*, 1994] assumed that annual cycles in SST at the equatorial Pacific and Atlantic stem from the same mechanism: a mixed-layer mode, in which the atmosphere and SST are locally coupled, with only ocean mixed-layer dynamics controlling SST. However, ocean dynamics display very different seasonal cycles in these two tropical basins. In the Pacific, thermocline depth has very weak variations on seasonal time scales and plays little role in the SST annual cycle [*Chang and Philander*, 1994; *Xie*, 1994]; while in the Atlantic, it has very pronounced variations and probably is the main factor in the heat budget of the SST annual cycle [*Houghton*, 1983; *Philander and Pacanowski*, 1986]. *Foltz et al.* [2003] showed that zonal advection is also important for the annual cycle of SST. Different ocean dynamics and heat budgets on seasonal time scales show that different mechanisms from that in the Pacific operate in the annual cycle of SST in the equatorial Atlantic. The latter is poorly simulated by state-of-the-art coupled climate models, limiting seasonal forecast skill in the Tropical Atlantic [*Stockdale et al.*, 2006]. Therefore, it is of practical interests to study the seasonal cycle of ocean dynamics in the Tropical Atlantic.

On interannual time scales, the zonal mode (or Atlantic Niño) [*Xie and Carton*, 2004; *Zebiak*, 1993] dominates variability in the Equatorial Atlantic. It arises from similar coupled ocean-atmosphere interaction to ENSO, although each of its three elements explain less variance than in the Pacific [*Keenlyside and Latif*, 2007]. Associated SST anomalies can exceed 1°C in the Atlantic cold tongue (20°W and 0°W, 6°S and 2°N). Although much weaker than the El Niño Southern Oscillation (ENSO), the zonal mode has major socio-economic impacts, exerting a significant influence on surrounding countries [*Carton and Huang*, 1994]. The zonal mode also displays different seasonality from ENSO. In the Pacific, ENSO often peaks

in boreal winter; while in the Atlantic, zonal mode events primarily peak in boreal summer [*Keenlyside and Latif*, 2007], but similar variability is also found in November-December [*Okumura and Xie*, 2006]. The seasonality of the zonal mode is most likely caused by the seasonal cycle of thermocline depth and atmospheric sensitivity to SST [*Keenlyside and Latif*, 2007; *Okumura and Xie*, 2006]. Despite similarities to ENSO in terms of the Bjerknes positive feedback, the existence of a delayed negative feedback has not been extensively investigated and deserves further study.

The influence of Atlantic zonal mode is not limited to surrounding countries, but extends to the Tropical Pacific [*Jansen et al.*, 2009; *Losada et al.*, 2009; *Wang*, 2006; *Wang et al.*, 2009], and even possibly to the Indian Ocean [*Kucharski et al.*, 2008; *Wang et al.*, 2009]. *Wang* [2006] found that Tropical Atlantic and Pacific SST anomalies form an inter-basin gradient and a positive feedback with the overlying Walker Circulation, indicating a coupled interaction between the two Tropical ocean basins. *Losada et al.* [2009] studied the response to the Tropical Atlantic SST anomalies using four AGCMs. Their results show that the SST anomalies produce a Gill-type response, which extends into the eastern Tropical Pacific. Using observation and reanalysis, *Rodríguez-Fonseca et al.* [2009] showed that since 1970, the warm phase of the Atlantic zonal mode in boreal summer favours the cold phase of ENSO in boreal winter and vice versa. They proposed the following mechanism: atmospheric anomalies induced over the Pacific by the Atlantic zonal mode influence the positive Bjerknes feedback there in boreal summer, and hence the development of ENSO. However, they were not able to fully verify this mechanism in tailored coupled model experiments, and thus the true mechanism coupling both basins remains uncertain.

In summary, although Tropical Atlantic and Pacific annual-to-interannual variability share similarities, differences exist and uncertainty exists in the true mecha-

nisms behind Tropical Atlantic variability. In addition, the Tropical Atlantic is not isolated, but is influenced by, and may influence climate variability in other Tropical oceans. Due its socio-ecnoimic impacts and as it forms an integral component of Tropical Climate variability, it is therefore important to better understand Tropical Atlantic variability. In this work, the following three aspects are addressed:

- In chapter 2, the dynamics of the mean seasonal cycle in the equatorial Atlantic are investigated, through analysis of observations and ocean model simulations. Certain aspects in the seasonal cycle of ocean dynamics are still not well understood. For instance, regarding the effects of equatorial waves on the seasonal cycle in thermocline depth and sea level, there exist two contradicting views, one based on equatorial wave dynamics [*Schouten et al.*, 2005] and the other on the recharge oscillator mechanism [*Bunge and Clarke*, 2009]. A second aspect is the effects of nonlinear dynamics on equatorial surface zonal currents (SEC), whose seasonal cycle at the equator cannot be explained by linear dynamics [*du Penhoat and Treguier*, 1985]. A third aspect is the prominent semi-annual cycle in surface zonal currents, thermocline depth and sea level, that occurs despite a comparatively weak semi-annual cycle in surface winds.

- Chapter 3 investigates the existence of a delayed negative feedback in Atlantic zonal mode, which is necessary for oscillatory behavior, but has not been extensively investigated [*Zebiak*, 1993; *Jansen et al.*, 2009]. In addition, despite similarities to ENSO, predictability potential of the Atlantic zonal mode has not been demonstrated and deserves more study.

- In chapter 4, the influence of the Atlantic zonal mode on ENSO is addressed using the Max-Planck-Institute (MPI) coupled model ECHAM5/MPI-OM (IPCC version). It has been hypothesized that the Atlantic zonal mode influences ENSO through impacting the Bjerknes positive feedback [*Rodríguez-Fonseca*

et al., 2009]. The latter plays an essential role for ENSO and a possible means to amplify small external influences. Therefore, a climate model with correct ocean-atmosphere coupling mechanisms in the tropical Pacific is required to study the influence of Atlantic zonal mode on ENSO. Such a study using coupled model with convincing results is still outstanding.

Chapter 2

Seasonal cycle in the upper Equatorial Atlantic Ocean

Abstract

The dynamics of the seasonal cycle in the upper equatorial Atlantic ocean are studied using observations and a hierarchy of ocean models. Distinctive features of the seasonal cycle are strong annual and semi-annual components; eastward (westward) propagating sea surface height (SSH) and thermocline depth at the equator (off the equator); and westward propagating surface zonal currents at the equator. Modelling results show that linear theory can explain the seasonal cycle in thermocline depth and SSH. While to first order linear theory can also explain the structure of the seasonal cycle of surface zonal currents at the equator, nonlinear terms are required: they weaken the variability and improve its phase and zonal extent. The important terms are meridional and vertical advection, and vertical diffusion of zonal momentum.

The linear solution is essentially determined by the four gravest baroclinic modes, and Kelvin and first meridional mode Rossby waves. The eastward propagation in thermocline depth at the equator results from the Kelvin wave contribution, while the westward propagation in thermocline depth off the equator and surface zonal

currents at the equator result from the first meridional mode Rossby wave. The contribution of Kelvin and Rossby waves generated by boundary reflections equals that of the directly forced waves. The semi-annual cycle in zonal winds although much weaker than the annual component forces a strong semi-annual component in SSH and surface zonal currents, because it excites the basin mode of the second baroclinc mode. This explains the observed feature in the seasonal cycle from March to August.

2.1 Introduction

In the equatorial Atlantic, sea surface temperature (SST) variability is dominated by the seasonal cycle, while interannual fluctuations are comparatively weak [*Xie and Carton*, 2004]. This picture contrasts that in the Pacific, where interannual variability and the annual cycle are of similar strength. While interannual variability in both basins is tightly phase locked to the seasonal cycle, it is to different seasons: In the Atlantic (Pacific) variability is strongest in boreal summer (winter). The seasonal cycle of SST in both basins, although exhibiting similarities in phase and strength (Fig. 2.1c, d), display distinct relationships to zonal wind stress (Fig. 2.1a, b). In the Pacific, SST and zonal wind stress variations are consistent with mixed-layer mode [e.g., *Chang and Philander*, 1994; *Xie*, 1994], but they are not in the Atlantic. These differences may at first seem quite surprising, given that the equatorial annual cycle and interannual variability interact with each other [e.g., *Tziperman et al.*, 1994; *Chang et al.*, 1995; *Liu*, 2002; *Keenlyside and Latif*, 2007], and if as previously assumed the mechanisms for the seasonal cycle in both basins are the same [e.g., *Chang and Philander*, 1994; *Xie*, 1994]. The seasonal cycle of ocean dynamics are, however, very different (Fig. 2.1e-h): In the Atlantic, thermocline depth [*Houghton*, 1983; *Philander and Pacanowski*, 1986; *Xie and Carton*, 2004] and surface zonal current [*Foltz et al.*, 2003] variations are both strong, while

in the Pacific thermocline variations are relatively weak [*Yu and McPhaden*, 1999]. Furthermore, in the Atlantic both quantities exhibit strong annual and semi-annual components, whereas in the Pacific the annual harmonic dominates. The SST, thermocline depth and zonal current fluctuations also exhibit quite different relationships in the Atlantic and Pacific, as are the seasonal heat-budget of the mixed-layer [e.g., *Wang and McPhaden*, 1999; *Foltz et al.*, 2003]. The aim of this paper is to better understand the dynamics of the seasonal cycle in the Atlantic.

Great progress has been made in understanding seasonal variations in the Atlantic of thermocline depth and dynamic height through analyzing observations and a wide range of modeling studies, including linear vertical (single and multiple) mode, reduced-gravity, and primitive equation models [e.g., *Adamec and O'Brien*, 1978; *Busalacchi and Picaut*, 1983; *du Penhoat and Treguier*, 1985; *du Penhoat and Gouriou*, 1987; *Philander and Pacanowski*, 1986; *Weisberg and Tang*, 1983; 1985; 1987; 1990]. However, certain aspects are still not well understood. One is that sea surface height propagates eastward at the equator and westward off the equator, as shown by *Schouten et al.* [2005]. They argued that equatorial waves produce these propagation features. However, *Bunge and Clarke* [2009] found a discrepancy between theoretical Kelvin waves phase speeds and the eastward propagation of sea level along the equator during boreal summer. Therefore, they argue that the latter is best explained as the interaction between two independent (empirical orthogonal function) modes that describe a recharge-discharge of equatorial heat content (analogous to the mechanism proposed by *Jin* [1997] for El Niño).

A second aspect is the effects of nonlinear dynamics on equatorial surface zonal currents. According to observed data (mainly SEQUAL/FOCAL field and historical ship drift), surface zonal currents also display robust seasonal variations [*Molinari*, 1983; *Richardson and McKee*, 1984; *Reverdin and McPhaden*, 1986; *Richardson and Walsh*, 1986; *Philander and Pacanowski*, 1986; *Richardson and Reverdin*, 1987;

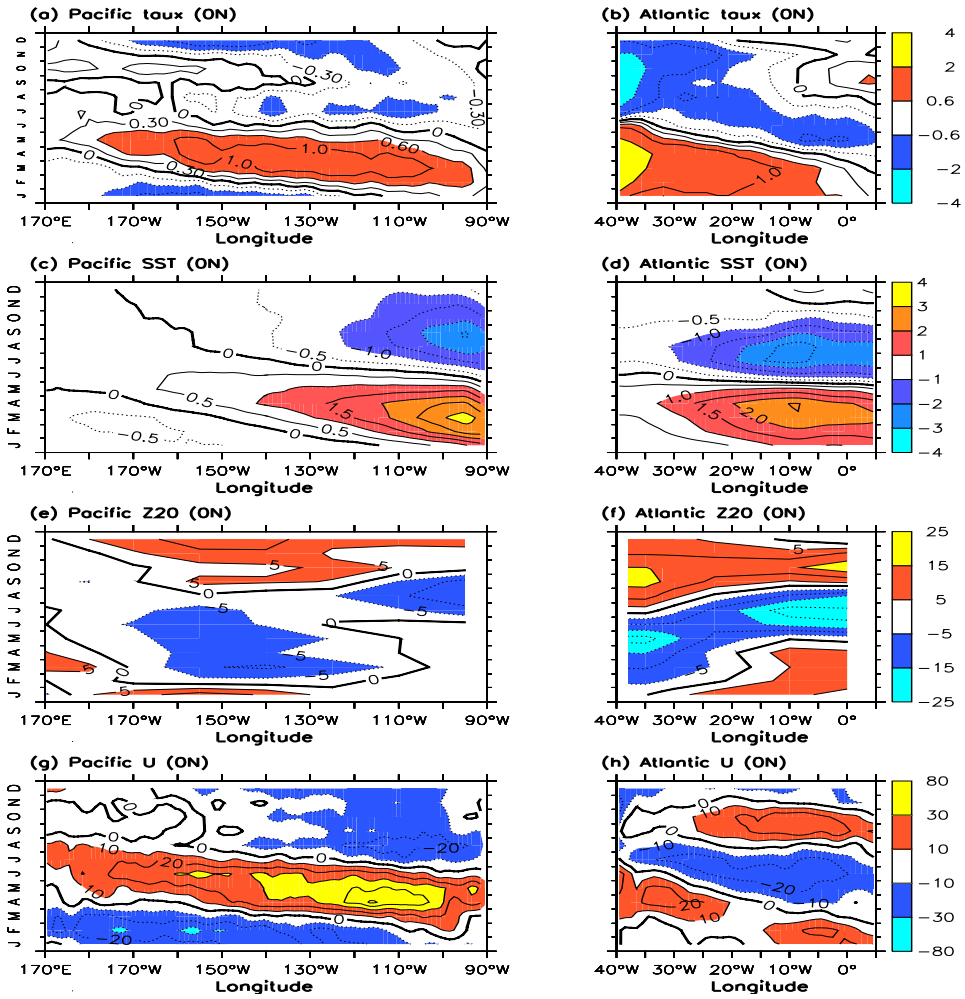

Figure 2.1: Seasonal cycle of (a,b) zonal wind stress (taux) (c,d) sea surface temperature (SST) and (e,f) 20°C isotherm depth (Z20) and (g,h) surface zonal currents at the equator in the Pacific and Atlantic. Anomalies with respect to the annual mean are shown. Wind stress are from the NCEP/NCAR reanalysis [*Kalnay et al.*, 1996]. SST are from NOAA [*Reynolds et al.*, 2002], and surface zonal currents are from OSCAR [*Bonjean and Lagerloef*, 2002]. The 20°C isotherm depth in the Pacific and Atlantic are from the TAO [*McPhaden et al.*, 1998] and PIRATA [*Servain et al.*, 1998], respectively. The contours for zonal wind stress are -2, -1, -0.6, -0.3, 0, 0.3, 0.6, 1, 2 ($\times 10^{-2} Nm^{-2}$). Contour interval of SST, Z20 and surface zonal currents are $0.5°C$, $5m$ and $10cms^{-1}$, respectively.

Richardson et al., 1992; *Arnault et al.*, 1999], especially the western North Equatorial Counter-Current (NECC) and equatorial branch of the South Equatorial Currents (SEC). *du Penhoat and Treguier* [1985] showed that linear dynamics can simulate the seasonal variability in NECC, but not in the equatorial branch of SEC. They speculated that the failure in simulating SEC is probably due to nonlinear dynamics, for instance vertical advection [*Philander and Pacanowski*, 1980].

A third aspect is the prominent semi-annual cycle in surface currents and SSH, occurring despite a comparatively weak semi-annual cycle in surface winds (Fig. 2.1b). Here it is argued that this feature results from the excitation of a basin mode (i.e., a free solution of equatorial ocean dynamics). Physically, the basin mode can be related to the circuit of a disturbance about the basin associated with the Kelvin and first meridional Rossby waves [*Cane and Moore*, 1981]. In the Atlantic, the period of the basin mode of the second baroclinic modes is 220 days and close to semi-annual. A similar argument was previously used to explain the strong semi-annual signal in the deep tropical Atlantic [*Thierry et al.*, 2004].

In this study, we investigate the dynamics of the mean seasonal cycle in the equatorial Atlantic, addressing the specific issues raised above. We mainly rely on analysis of observations and ocean model simulations forced with observed winds. The remainder of this paper is as follows. Section 2.2 describes the observations and models used in this study. Section 2.3 presents the observed mean seasonal cycle. In sections 2.4, a hierarchy of ocean model simulations are presented and used to explain the dynamics of the seasonal cycle, including its phase propagation features.

2.2 Data and model

In this study, the mean seasonal cycle is computed from a suite of satellite and in-situ observations, and reanalysis. Except where otherwise mentioned, the period

considered is 1993 to 2007, and only anomalies with respect to the annual mean are shown.

Monthly mean NOAA optimum interpolation (OI) SST V2 are used here from the NOAA/OAR/ESRL PSD, Boulder, Colorado, USA (http://www.cdc.noaa.gov/). The SST analysis is produced weekly on a one-degree grid, using in situ and satellite SST. Before the analysis is computed, the satellite data is adjusted for biases using the method of *Reynolds* [1988] and *Reynolds and Marsico* [1993]. The NOAA OI.v2 SST monthly fields are derived by a linear interpolation of the weekly fields to daily fields then averaging the daily values over a month.

Thermocline depth is defined as the depth of the 20°C isotherm. It is computed from temperature data from the Pilot Research Moored Array in the Tropical Atlantic [PIRATA; *Servain et al.* [1998]] at four locations along the equator: 35°W, 23°W, 10°W, and 0°W. At 0°W and 10°W data are not continuous, but in total there are about seven and five years of data, respectively. At 23°W and 35°W, data records are about 9 years long and continuous. As interannual variability is weak in comparison to the seasonal cycle, the data although short are sufficient to describe the seasonal cycle. To calculate the mean seasonal cycle, daily mean time series are averaged to monthly means. Off the equator, PIRATA data are insufficient to describe the seasonal cycle. Thus, AVISO SSH products are employed. In the tropics, SSH and thermocline depth variations are closely related. These data are from the Topex/Poseidon and ERS satellites and are available since 1992.

The OSCAR surface currents are derived from gridded SSH, surface wind, and SST data, using a combination of the geostrophic, Ekman-Stommel, and thermal-wind approximations, with a special treatment of the equatorial singularity [*Bonjean and Lagerloef*, 2002]. The data compare favorably with drifter data and in situ observations. In addition to the OSCAR data, a drifter-derived climatology of global near-surface currents are also used [*Lumpkin and Garraffo*, 2005].

Three models are used in this study. The first is a global state-of-the art ocean general circulation model (OGCM), the Max-Planck-Institute for Meteorology Ocean Model (MPI-OM) [*Marsland et al.*, 2003]. The model is forced with the NCEP/NCAR reanalysis [*Kalnay et al.*, 1996] for the period 1950 to 2001, using standard bulk formulas for the calculation of heat fluxes and a weak relaxation of surface salinity to the *Levitus and Boyer* [1994] climatology. Here only the period 1986-2000 is considered.

The second model is an intermediate ocean model (IOM) designed to simulate the dynamical response of the equatorial ocean to wind forcing [*Keenlyside*, 2001; *Keenlyside and Kleeman*, 2002]. The model consists of linear and nonlinear components. The linear component is basically the model of *McCreary* [1981], but takes into account horizontally varying background stratification. It consists of ten baroclinic modes plus two surface layers. The two surface layers are governed by Ekman dynamics and represent baroclinic modes 11-30. The nonlinear component is a simplified treatment of the residual equations of motion (i.e., after removing linear terms) for zonal momentum and is solved in the two surface layers. These nonlinear terms are important in the surface zonal momentum budget in the equatorial Atlantic [*Philander and Pacanowski*, 1980], which cannot be fully described by linear dynamics [*du Penhoat and Treguier*, 1985]. Linear and nonlinear components are calculated independently so that their contributions can be investigated separately. Model equations and parameters are fully described by *Keenlyside* [2001].

The model is configured for the Atlantic basin between 30°S-30°N and takes into account realistic coasts, where the no slip lateral boundary condition is applied. An Arakawa c-grid is used with 2 degree zonal grid spacing, and a stretched meridional grid, with 0.5 degree grid spacing within 10 degrees of the equator, extending to 3 degrees at the boundaries. The vertical grid has 31 levels with 8 levels in the surface 125m and a 4500m flat bottom. The two surface Ekman layers cover the upper 125m

and are divided by the mixed layer depth. The model is integrated using a standard leapfrog scheme, with a time step of 5000 seconds, and filtering every 60 time steps. The model is forced only by surface wind stress from the NCEP reanalysis [*Kalnay et al.*, 1996] for the period 1980 to 2007. The period 1993 to 2007 is considered here. The baroclinic modes and corresponding shallow water speeds are calculated from the Levitus climatological temperature [*Locarnini et al.*, 2006] and salinity [*Antonov et al.*, 2006] data.

The third model is a simple meridional mode model of the first four baroclinic modes, and is essentially the model of *Gill and Clarke* [1974]. It is used to decompose the linear solution of the IOM into Kelvin and Rossby waves and to investigate the contribution of boundary reflections. Model parameters are chosen to match those of the IOM. The long wave approximation is taken, filtering out high-frequency inertia-gravity and short Rossby waves. In addition, meridional wind stress is neglected, as it is relatively inefficient at exciting a dynamical response in the equatorial ocean on seasonal timescales [*Gent et al.*, 1983; *Yu and McPhaden*, 1999]. The eastern and western boundary conditions are $u = 0$ and $\int_{y_s}^{y_n} u\,dy = 0$, respectively. The latter accounts for the fact that short Rossby waves are filtered from the solution [*Cane and Sarachik*, 1981]. The model domain extends from 45°W to 5°E in longitude, but is unbounded meridionally. The influence from the Gulf of Guinea and Brazilian coast on the propagation of planetary waves at the equator is assumed negligible. This assumption is not made in the other two models, but appears reasonable as this model can reproduce the key features simulated by those models. *Weisberg and Tang* [1983; 1985; 1987; 1990] also made the same assumption and were successful in reproducing many features of seasonal variations of the thermocline at the equator. The zonal wind stress used to drive the model is the climatologically monthly mean of the NCEP reanalysis [*Kalnay et al.*, 1996] from 1993 to 2007. The model is run for three years and only the third year is analyzed, when the simulated seasonal variations have stabilized. Calculations are limited to the Kelvin and first meridional

mode Rossby waves.

2.3 Observed seasonal cycle

In the western Atlantic the seasonal cycle in zonal wind stress (Figure 2.1b) is dominated by an annual cycle, while in the east a semiannual cycle is apparent. In April, westward stress firstly appears in the eastern part and then moves westward [*Picaut*, 1983]. In contrast to zonal winds, the meridional wind stress (not shown) does not exhibit a semi-annual component.

The annual mean equatorial thermocline slopes upward toward the east, and is around 100 m in the west and 50 m in the east (not shown). An interesting aspect is that seasonal variations have larger amplitude on the eastern and western sides of the basin, rather than at the center and are about 90° out of phase from March to July (Figure 2.1f), which is reminiscent of the basin mode [*Cane and Moore*, 1981]. In the west the annual cycle is dominant, with minimum (maximum) depth occurring in May (September). These variations are mainly a direct response to zonal wind stress (Figure 2.1b) [*Philander and Pacanowski*, 1986]. In April and May, the thermocline is most close to surface in the western Atlantic, responding to the relaxation in zonal winds (Figure 2.1b). The shallow thermocline in April-May progresses eastward and reaches the Gulf of Guinea in boreal summer, when the thermocline depth there decreases by almost half (not shown). These changes are closely related to the rapid decrease in SST there (Figure 2.1d). The deepening of the thermocline in the west in September also propagates eastward, but the propagation is much more rapid than for the shoaling (Figure 2.1f). Towards the east a semiannual cycle also appears in the thermocline variability, and in the far east it is almost as strong as the annual cycle. In the tropics sea-level and thermocline variations are closely related, and the observed sea-surface variations at the equator (Figure 2.2a) corroborate the picture from PIRATA.

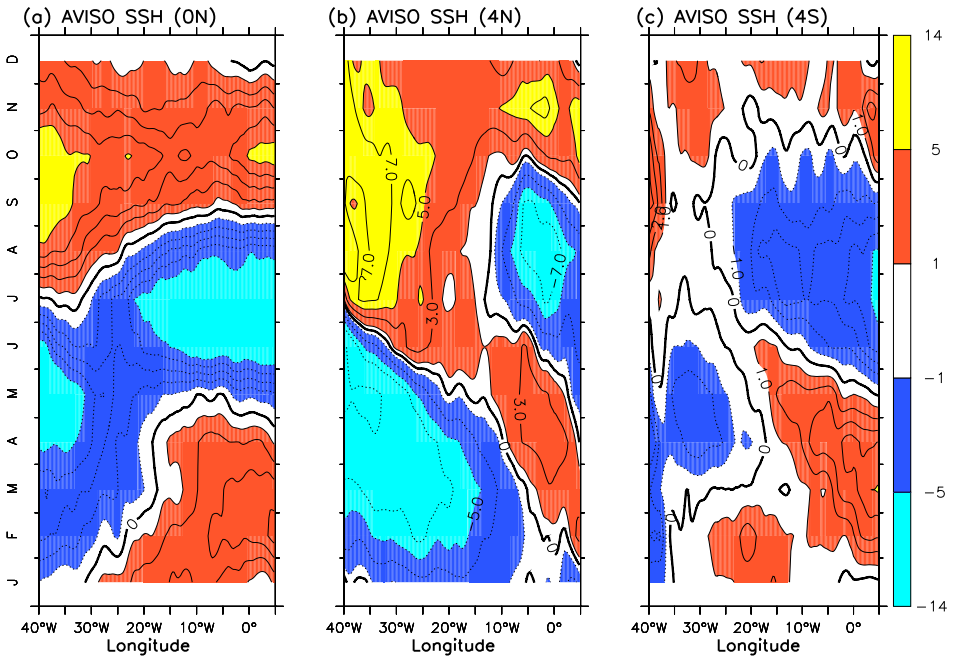

Figure 2.2: Seasonal cycle of sea surface height (SSH) at the (a) equator, (b) 4°N and (d) 4°S. Anomalies with respect to the annual mean are shown. SSH are from AVISO (http://www.aviso.oceanobs.com/). Contour interval of SSH at the equator and 4°S is 1cm. Contours of -12,-7,-5,-3,-1,0,1,3,5,7,12(cm) are shown for SSH at the 4°N.

Off the equator, SSH also exhibit a pronounced seasonal cycle (Figure 2.2b, c), with significant annual and semi-annual cycles in the west and east, respectively, similar to that at the equator. The seasonal cycle contributes to over a half of the total variability in SSH [*Schouten et al.*, 2005]. In contrast to that at the equator, SSH variations off the equator propagate westward. As mentioned above, PIRATA data are insufficient off the equator to describe seasonal variations in thermocline depth. WOA05 climatological monthly ocean temperature data [*Locarnini et al.*, 2006] show variations consistent with the satellite SSH data off (and at) the equator (not shown).

The seasonal cycle of surface zonal currents along the equator in the Atlantic is dominated by a semiannual cycle and is strongest in the central part of the basin

(Figure 2.1h) [*Richardson and McKee*, 1984]. Seasonal variations propagate westward along the equator during the first half of calendar year. At the beginning of the year, the zonal current anomaly is eastward (weak and westward) in the east (west). The eastward anomaly then propagates westward, reaching 35°W in April and May. In the east when zonal wind stress strengthens in April (Figure 2.1b), the eastward zonal currents anomaly reverses sign and propagates westward along the equator. Enhanced zonal currents persist until about August. Before August, seasonal variations of zonal currents and zonal wind stress along the equator have similar phase, direction, and propagation characteristics [*Richardson and McKee*, 1984]. After August, zonal current anomaly is eastward in September and October. The eastward anomaly extends almost simultaneously across the whole equatorial Atlantic, although the amplitude varies with longitude, being stronger between about 20°W and 0°W. The seasonal cycle of zonal currents at the equator from drifters (not shown), although very noisy and with stronger amplitude, corroborates the features seen in the OSCAR data.

The 90° out of phase relationship between east-west gradient of sea level and surface zonal currents from March to August (Fig. 2.3a) also shows signs of the basin mode. At the peak of the positive phase (Fig. 2.3b), the zonal currents are weak and the zonal east-west gradient is at its maximum. The gradient drives westward currents that in turn weaken the gradient. The currents are strongest during the transition phase (Fig. 2.3c), when the gradient is almost zero. The signal of the basin mode is clear from March until about August and then becomes less clear (Fig. 2.3a).

2.4 Dynamics of the seasonal cycle

The dynamics of seasonal cycle are now investigated using the three models. Both the OGCM and IOM reproduce the seasonal cycle in SSH on and off the equator well

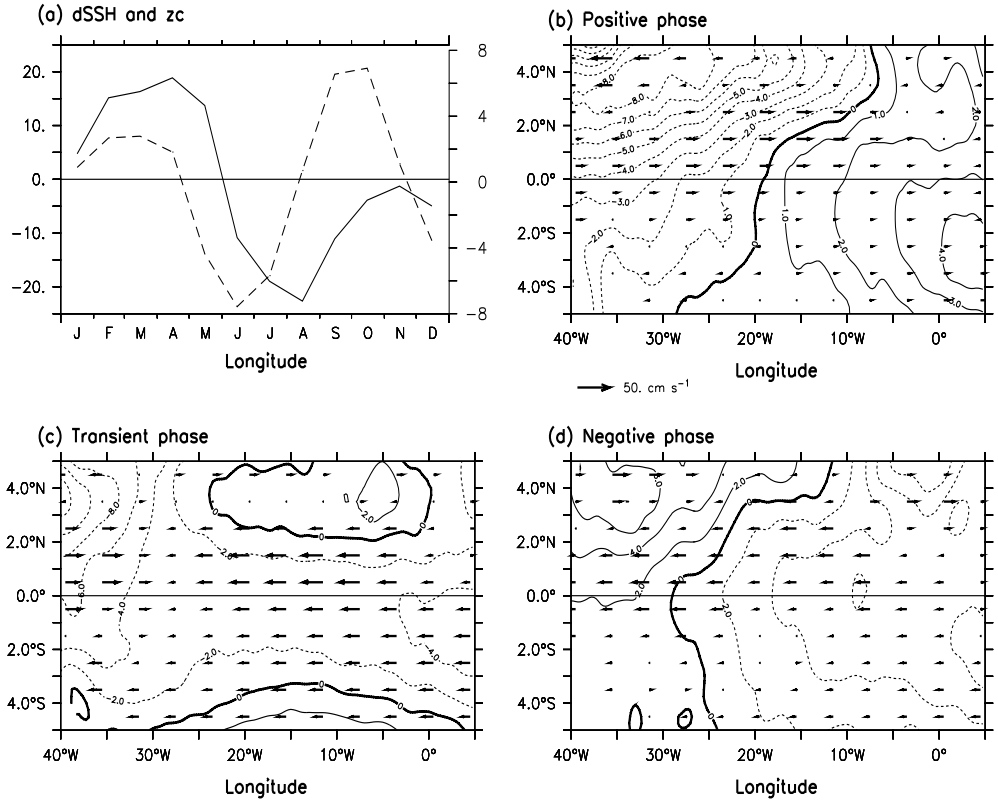

Figure 2.3: (a) The seasonal variations of east-west gradient of SSH (solid) and surface zonal currents (dashed). Here, east-west gradient denotes the difference between SSH averaged from 15°W to 5°E and SSH averaged from 45°W to 25°W at the equator, and surface zonal currents are averaged from 25°W to 10°W at the equator. (b), (c) and (d) SSH (contours) and surface zonal currents (vectors) for positive (March, April), transient (May, June) and negative (July, August) phases, respectively. The contour interval is 1cm.

(Figure 2.4). In particular, at the equator the annual cycle in the west and semi-annual cycle in the east are simulated by both models (Figure 2.4a,d), including the rapid sea-level decrease in the cold tongue during boreal summer, and the basin-wide increase in sea-level in September and October. A deficiency of both models is that simulated SSH variations are too weak, and in the west they lead observations by about one month and are in phase with the zonal wind variations; a problem previously noted [*Philander and Pacanowski*, 1986]. The reasons for this deficiency are not clear, but may result from errors in the forcing data or in model physics. As

this region is directly under the ITCZ, the contribution of precipitation to sea level may be also important. Along 4°N, despite being generally too weak, both models (Figure 2.4b,e) reproduce the basic pattern of the seasonal cycle (Figure 2.2b): prominent annual and semi-annual cycles in the west and east, respectively. The westward propagation is also well reproduced. Along 4°S, both simulations (Figure 2.4c,f) also compare well to observations (Figure 2.2c). The westward propagation of the positive anomaly at the beginning of the year is as observed, but it is stronger and slightly phase shifted, especially in the west.

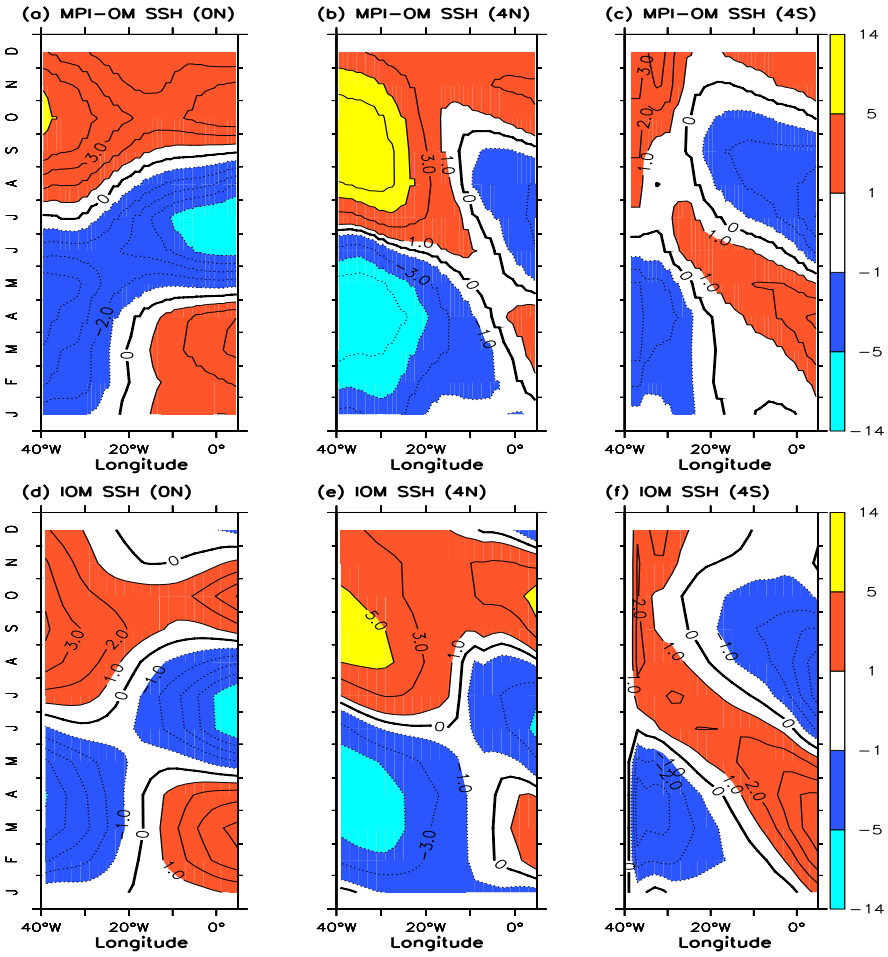

Figure 2.4: Seasonal cycle in SSH simulated by the MPI-OM and IOM at (a,d) the equator, (b,e) 4°N, and (c,f) 4°S. Anomalies with respect to the annual mean are shown with contours as in figure 2.2.

The seasonal cycle of the surface zonal currents at the equator is also simulated well by both models (Figure 2.5a,b), in terms of amplitude and structure. In particular, the models correctly simulate a semiannual cycle along the whole equatorial Atlantic, including the boreal summer westward currents anomalies and their westward propagation. Differences exist among the observations and the two model simulations, but they are of similar order to the differences between OSCAR (Figure 2.1h) and drifter (not shown) data. Another difference is that MPI-OM surface zonal currents display a westward propagation from September to December, but observed currents are almost stationary; however, this may be partly due to different periods considered (Section 2.2). Separating the IOM surface zonal currents into linear (Figure 2.5c) and nonlinear (Figure 2.5d) components, shows that the linear solution has a lot of resemblances to observations. In particular, the observed westward propagation and semi-annual cycle are captured, except in September and October when the linear solution is unable to reproduce the observed basin wide eastward currents anomalies. Another deficiency is that the strength of the currents in the linear component are too large (about three times the observed strength) consistent with previous work [*du Penhoat and Treguier*, 1985]. Comparing total, linear and nonlinear surface zonal currents (Figure 2.5b,c,d), shows that the nonlinear terms have equal magnitude to linear terms and play an important role. They weaken the linear terms and lead to realistic zonal currents strength and they also cause the eastward currents anomaly to extend along the entire equator in September and October. Thus, the nonlinear terms provide a necessary correction to the linear solution, contributing significantly to the strength and phase of simulated currents.

The terms in the nonlinear equations are zonal, meridional and vertical advection of zonal velocity and horizontal and vertical diffusion of nonlinear zonal velocity. The most significant terms are meridional advection, vertical diffusion, and vertical advection; zonal advection is negligible (Figure 2.6). The driving terms are meridional and vertical advection, while vertical diffusion dissipates nonlinear velocity.

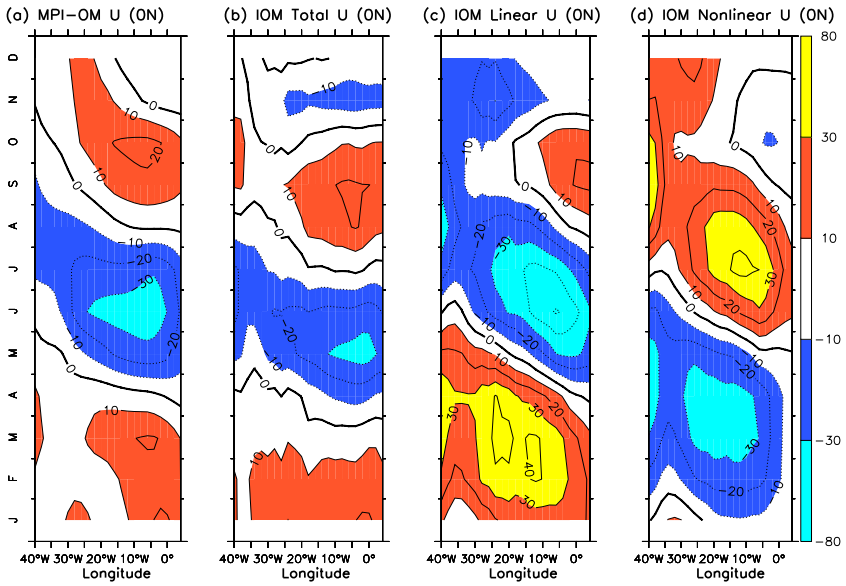

Figure 2.5: Simulated seasonal cycle of surface zonal currents at the equator, (a) MPI-OM (b) IOM total, and (c) IOM linear and (d) IOM nonlinear components. Anomalies with respect to the annual mean are shown with contours as in figure 2.1h.

Meridional advection, which is related to variations in both meridional currents and meridional variation of zonal currents, is strong (weak) from June to October (January to May). Vertical advection is controlled by changes in upwelling, which follow changes in zonal wind (Figure 2.1b). In boreal summer, for example, when upwelling is stronger following the intensification of the surface trades, vertical advection of momentum brings more eastward momentum to the surface layer and reduces the westward momentum. This is consistent with *Philander and Pacanowski* [1980].

To better understand the linear solution, it is decomposed into (vertical) baroclinic modes, Kelvin and Rossby waves, and contributions from eastern and western boundary reflections. The seasonal cycle of SSH and surface zonal currents in the linear solution is determined primarily by the first four baroclinic modes (not shown). For SSH, the second mode is dominant, but for surface currents the second and third ones are most important. These results are consistent with previous studies

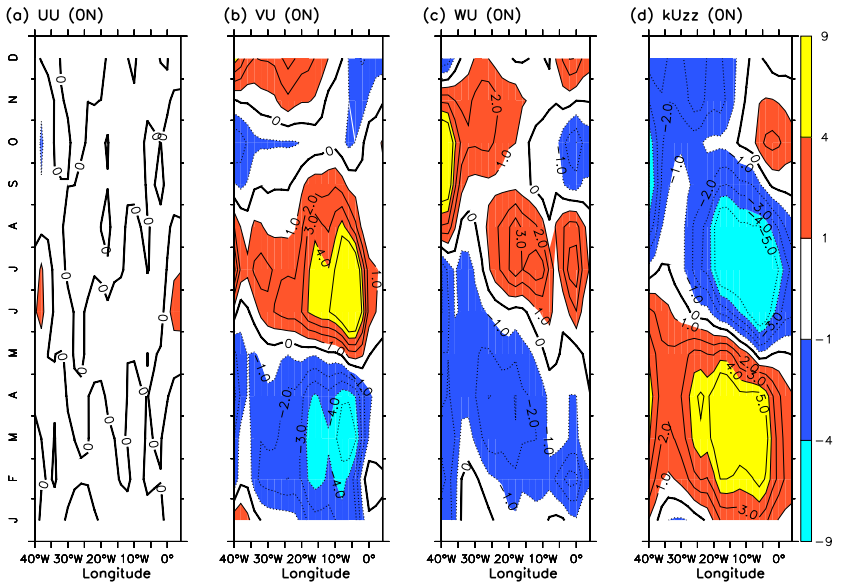

Figure 2.6: Seasonal cycle of the zonal momentum budget of the nonlinear component of the IOM, (a) zonal advection, (b) meridional advection, (c) vertical advection, and (d) sum of vertical and horizontal diffusion of zonal momentum. The contour interval is $10^{-5} cms^{-2}$.

[*du Penhoat and Treguier*, 1985; *Illig et al.*, 2004; *Thierry et al.*, 2004; *Brandt and Eden*, 2005].

The wind forced meridional mode model, which includes only the first four baroclinic modes, and the Kelvin and first meridional mode Rossby waves, is able to reproduce the essential features of the seasonal cycle in SSH (Figure 2.7a). At the equator, the eastward propagation of sea level occurring between January and August is captured. As are the more rapidly eastward propagating, basin wide SSH anomalies that occur in September and October. The contribution of Kelvin (Figure 2.7b) and Rossby (Figure 2.7c) waves to the solution is comparable in the west, but in the east the Kelvin wave contribution is about three times larger. The Kelvin wave component (Figure 2.7b) gives rise to the eastward propagation in SSH. At eastern and western boundaries, Kelvin and Rossby wave contributions are in phase with each other, indicating the importance of boundary reflections [*Schouten et al.*,

2005]. There are some differences between simulated and observed SSH variations. For example, at the end of the year in the east, a negative signal is simulated, while a positive one is observed. Simulated variability in the west is also stronger than observed.

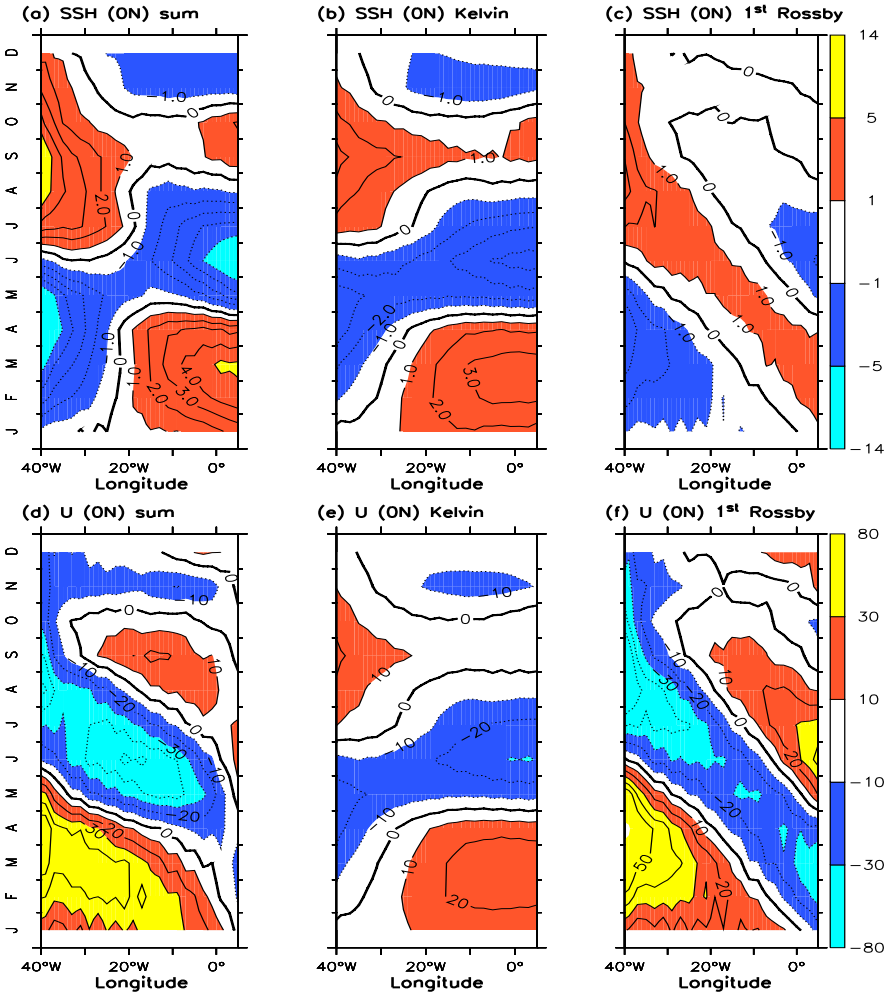

Figure 2.7: The contribution of (a,d) the sum of Kelvin and 1st Rossby waves, (b,e) Kelvin waves, and (c,f) 1st Rossby waves to the seasonal cycle of SSH (upper) and surface zonal currents (lower) at the equator. Contour of SSH and surface zonal currents are as in figures 2.2 and 2.1, respectively.

For surface zonal currents at the equator, the meridional mode model (Figure 2.7d) essentially reproduces the results of the linear component of the IOM (Figure 2.5c). The Kelvin (Rossby) wave zonal currents anomaly is, by definition, pro-

portional to the Kelvin (Rossby) wave SSH anomaly. However, the Rossby wave contribution (Figure 2.7f) is now greater than that of the Kelvin wave (Figure 2.7e). This is because at the equator the first meridional Rossby wave contributes proportionally more to surface zonal currents than SSH anomalies (e.g., *Gill* [1982]). Thus, the Rossby wave contribution (also forced by westward propagating zonal wind stress) gives rise to the westward propagation in surface zonal currents at the equator. *Yu and McPhaden* [1999] reached a similar conclusion for the Pacific.

At 4°S and 4°N, the amplitude of the second baroclinic mode Kelvin wave is only 20% of its equator maximum. Thus at these latitudes, Rossby waves dominate. The Rossby wave component (Figure 2.7c) for SSH resembles the average variations of observed SSH at 4°S and 4°N (not shown), which mainly result from meridionally symmetric long Rossby waves. Thus, the first meridional mode Rossby waves explain the westward propagation in observed sea-level at these latitudes.

The contribution of Kelvin and Rossby wave reflections at the eastern and western boundaries to the equatorial SSH and surface zonal currents variability is computed by the model (Figure 2.8). Their contribution to the seasonal cycle of simulated SSH and surface zonal currents at the equator equals that of the wind forced waves (not shown). This is consistent with previous studies [*Philander and Pacanowski*, 1986; *Schouten et al.*, 2005]. This is in contrast to the Pacific, where boundary reflections are not important [e.g., *Yu and McPhaden*, 1999].

As shown above, the seasonal cycle exhibits a strong semi-annual cycle and has features of the classical basin mode, whereas the dominant wind forcing is annual (Fig. 2.9a,b). The free oscillation (basin mode) of the second baroclinic mode has a period of 220 days [*Cane and Moore*, 1981]. To investigate whether it is excited and may explain these observed features, the meridional mode-model was forced separately with annual (Fig. 2.9a) and semi-annual (Fig. 2.9b) wind components. SSH and surface currents generated by the semi-annual wind forcing (Fig. 2.9d,f)

are similar in amplitude to those generated by the annual forcing (Fig. 2.9c,e). They also display the essential features of the basin mode: zonal SSH gradient and surface zonal current variations that are 90° out of phase. From March-August (September-February) the semi-annual and annual components constructively (destructively) interfere and the basin mode features are most (less) prominent in observations.

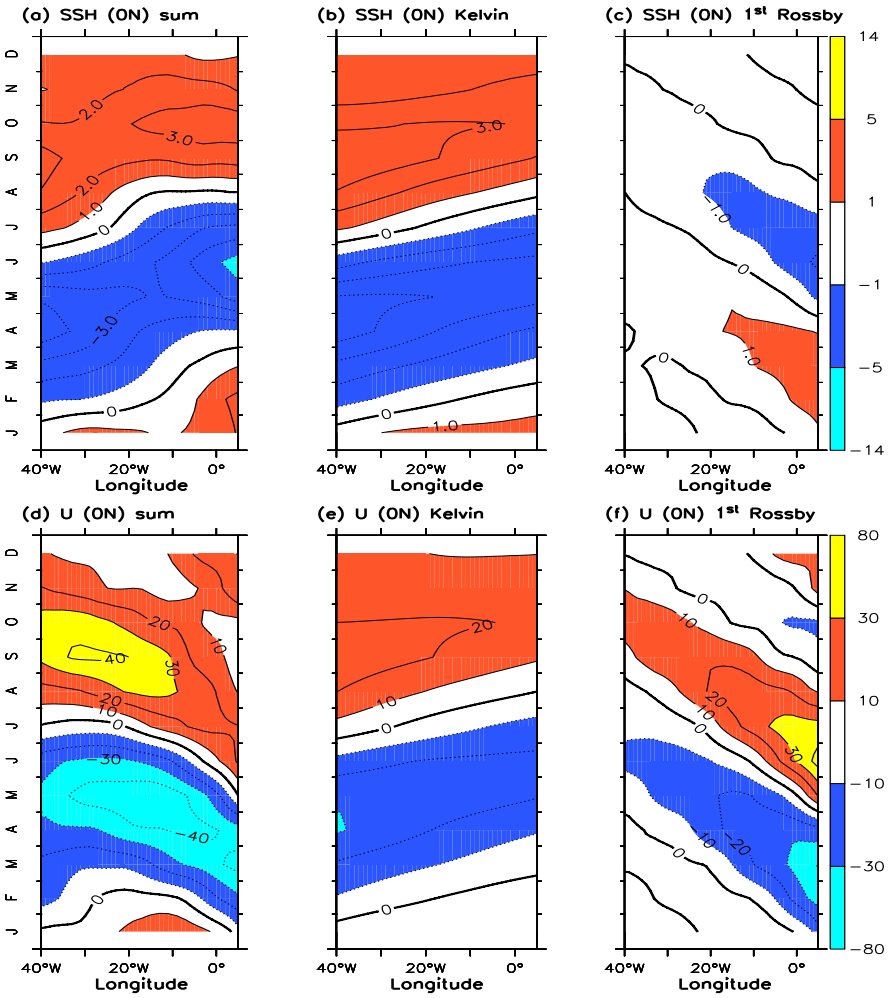

Figure 2.8: Contribution of boundary reflections to seasonal cycle of (upper) SSH and (lower) surface zonal currents at the equator as decomposed into (a,d) the sum of Kelvin and 1st Rossby waves (b,e) Kelvin waves and (c,f) 1st Rossby waves. Contour of SSH and surface zonal currents are as in figures 2.2 and 2.1, respectively.

We further investigate the contributions of wind-forced waves (Fig. 2.10a, c) and waves generated by boundary reflections (Fig. 2.10b, d) to sea level for semi-

annual (upper) and annual (lower) components, respectively. The direct response to the semi-annual component of wind stress is much weaker than that to annual component. Boundary reflections enhance (partly cancel) the responses to the semi-annual (annual) component of wind stress so that total semi-annual component (Fig. 2.9d) of sea level is comparable with annual component (Fig. 2.9c). Thus, the free-oscillation of second baroclinic mode appears responsible for the strong semi-annual cycle, despite a weak semi-annual wind forcing.

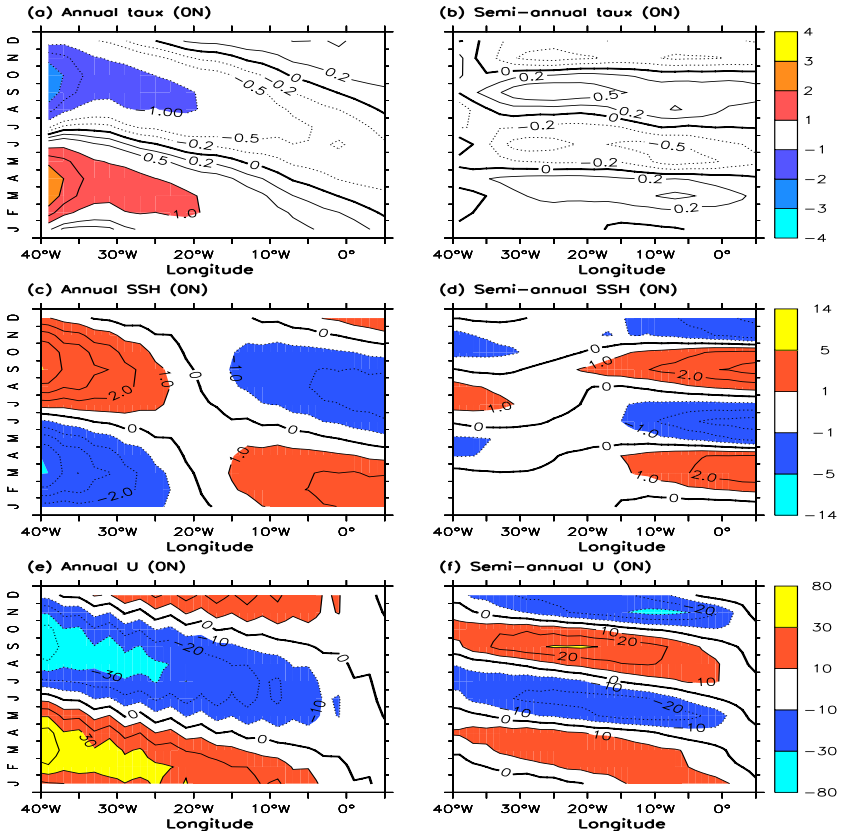

Figure 2.9: Annual harmonic (a) and residual semi-annual (b) components of NCEP/NCAR zonal wind stress [*Kalnay et al.*, 1996] and the corresponding SSH (c,d) and surface zonal current (e,f), as generated by the Kelvin and 1st Meridional Rossby waves. Contour interval of zonal wind stress (a,b)is $0.5 \times 10^{-2} Nm^{-2}$, with additional contours $-0.2 \times 10^{-2} Nm^{-2}$ and $0.2 \times 10^{-2} Nm^{-2}$. Contour interval of SSH (surface zonal currents) is $1cm$ ($10cms^{-1}$).

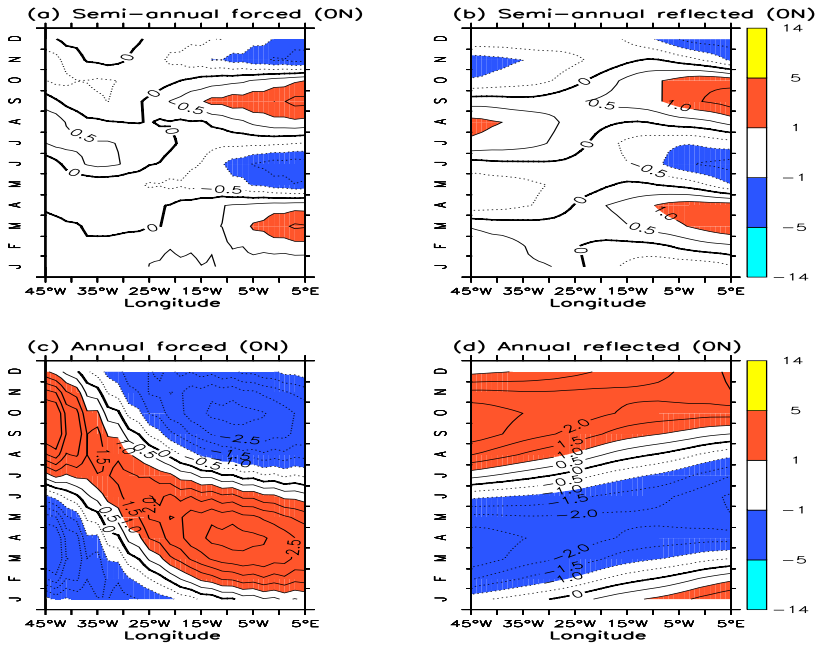

Figure 2.10: Contribution of wind-forced waves (a, c) and waves generated by boundary reflections (b, d) to SSH for semi-annual (upper panel) and annual (lower panel) zonal wind stress. Contour interval is 0.5 *cm*.

2.5 Discussions and conclusions

In this study, the seasonal cycle of surface wind, SST, SSH and surface zonal currents were first described using in-situ and satellite observations and atmospheric reanalysis primarily between 1993 and 2007. Seasonal variations in thermocline depth and sea level display prominent annual and semi-annual cycles in the west and east, respectively. At the equator, variations propagate eastward, but westward at 4°N and 4°S. Surface zonal currents at the equator exhibit a dominant semi-annual cycle with westward propagation. This description is consistent with previous studies and corroborated by other climatologies.

Although the seasonal cycle in the equatorial Atlantic has received much attention, several aspects remain debated. Here three of these are addressed, using an OGCM, an intermediate ocean model (IOM) and a linear meridional mode model.

First, what is the origin of the east-west propagation characteristics in SSH and zonal currents. The modelling results here show that linear dynamics can explain the phase and propagation characteristics in the seasonal variation of sea level and also get key features of surface zonal current variations. The linear solution is essentially reproduced by the first four baroclinic modes, although the second and third are dominant. Only the Kelvin and first meridional mode Rossby waves are required, with boundary reflected waves contributing as strongly as directly forced waves. For SSH at the equator, both Kelvin and Rossby wave contributions are significant, but the Kelvin wave contribution dominates and results in eastward propagation. At 4°N and 4°S, Rossby waves dominate variability and give rise to westward propagation. For surface zonal currents at the equator, the Rossby wave contribution is larger than that of the Kelvin wave, explaining the observed westward propagation. The coincidence of integrating characteristics of Rossby waves with westward propagating zonal wind stress enhances the westward propagating signal, consistent with *Weisberg and Tang* [1983]. However, Rossby waves related to the stationary semi-annual component of zonal wind stress and resulting mainly from eastern boundary reflections also contribute.

These results in many respects are not entirely new, being based in essence on the well established importance of long, nondispersive Kelvin and Rossby waves [*Cane and Sarachik*, 1981]. However, they provide a clear decomposition of the dynamics using modern forcing data. *Schouten et al.* [2005] found that sea level variations have the same westward phase speed as the first meridional mode Rossby of the second baroclinic mode at 4°N and 4°S. They are reflected as a Kelvin wave on the western boundary and propagate eastward through the whole basin in September and October at the equator. The modelling results here strongly support their arguments. *Bunge and Clarke* [2009] found that eastward propagation of sea level from April to July at the equator is too slow compared to theoretical phase speeds of Kelvin waves of the first few baroclinic modes. They did not consider variations

in September and October, nor did they find eastward propagation in zonal wind stress. Therefore, they excluded equatorial waves as an explanation [*Schouten et al.*, 2005]. However, modelling results here show that Kelvin and Rossby waves are both important at the equator. Additionally, the contributions of boundary reflections equal that of the wind-forced response. As a result of these factors, it is not possible to interpret the propagation speed in terms of single forced Kelvin wave [*Cane and Sarachik*, 1981].

The second aspect addressed was the role of non-linearity in the seasonal cycle of surface zonal currents at the equator. Although linear theory can explain the phase and east-west propagation of the latter, variations are far too strong. Here, nonlinear terms were shown to weaken the variability to observed levels, and improve its phase and zonal extent. The most significant terms are meridional advection, vertical diffusion, and vertical advection; zonal advection is negligible. Meridional and vertical advection drive changes in the nonlinear velocity. Vertical diffusion dissipates nonlinear velocity. In particular, vertical advection of momentum brings more eastward momentum to the surface layer and reduces the westward momentum in the cold tongue when upwelling is stronger in boreal summer. These results clarify the cause of deficiencies in linear models [*du Penhoat and Treguier*, 1985] and the importance of non-linearity [*Philander and Pacanowski*, 1980].

The third aspect investigated was the prominence of the semi-annual cycle in SSH and surface zonal currents that is unexpected given the dominance of the annual cycle in surface winds. Modelling results indicate that this occurs because the semi-annual cycle in surface winds resonantly excites the second baroclinic mode's basin mode. The basin mode (schematic in Fig. 2.11) is a free solution of equatorial ocean dynamics [*Cane and Moore*, 1981]. The period is set by the time it takes a disturbance to circuit the basin, and hence is dependent on the wave speed and basin size. For the second baroclinic mode in the Atlantic it is about 220 days,

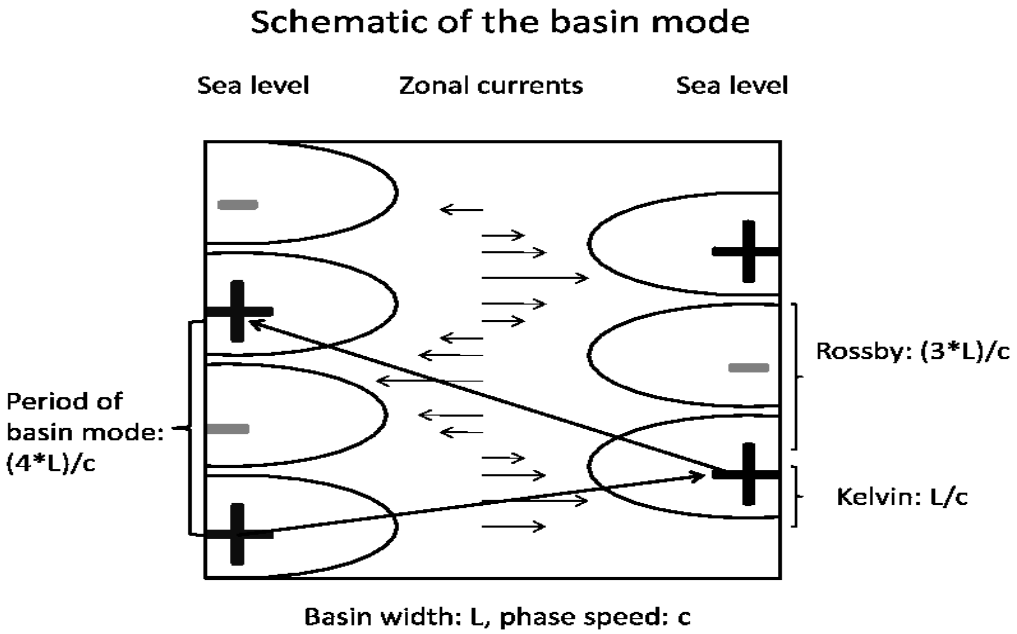

Figure 2.11: Schematic illustrating the basin mode [*Cane and Moore*, 1981].

which is approximately semi-annual. Thus, the semi-annual component in zonal wind stress, although much weaker than the annual component, is able to force a strong semi-annual cycle in SSH and surface currents. The result also explains why characteristic features of the basin mode features are apparent in the observed seasonal cycle. While a similar argument was given to explain the semi-annual signal in the deep tropical Atlantic [*Thierry et al.*, 2004], the role of the basin mode at the surface has not been previously recognized.

The results here were drawn from three models, which of course have deficiencies. For example, sea level variability, especially at 4°N, is slightly underestimated and not always in exact phase with observations in both the IOM and OGCM. In addition, the models used here are all low-resolution and do not capture Tropical Instability Waves, which are important in the Tropical Atlantic [*von Schuckmann et al.*, 2008]. However, the models used here are able to reproduce the key features of the observations, providing confidence in our results.

The results here have several interesting implications. First, they imply that although the seasonal cycle of SST in the equatorial Atlantic and Pacific are similar, the dynamics are likely very different. In particular, previous suggestions that the seasonal cycle in SST in the Atlantic results from a coupled atmosphere mixed-layer *SST-mode* not involving thermocline variations [*Chang and Philander*, 1994; *Xie*, 1994]. However, the seasonal relationship among SST, thermocline depth, and surface zonal currents in the Atlantic appear more consistent with a *thermocline-mode*. This difference maybe partly due to the different basin sizes. A different mechanism for the seasonal cycle in SST in the Atlantic has implications for the interaction of the seasonal cycle with interannual variability, and hence deserves further attention.

Acknowledgments

We thank Stephane Raynaud for providing the latest version of the IOM, and Peter Brandt and Verena Hormann for fruitful discussions. The work was supported by the European Union AMMA project, DFG Sonderforschungsbereich 754 project and the German BMBF Nordatlantik project.

Chapter 3

Equatorial Atlantic interannual variability: the role of heat content

Abstract

The dynamics of the Equatorial Atlantic zonal mode are studied using observed sea surface height (SSH), sea surface temperature (SST), and heat flux and reanalysis wind stress and upper ocean temperature. Principal oscillation pattern (POP) analysis shows that the zonal mode is an oscillatory normal-mode of the observed coupled system, obeying the delayed-action/recharge oscillator paradigm for ENSO. Variations in equatorial averaged SSH, a proxy for upper ocean heat content, precede SST anomalies in the cold tongue by 4-5 months, about a quarter of the POP period. Positive subsurface temperature anomalies appear in the west, as a delayed response to the preceding cold event. These propagate eastward, where due to the shallow thermocline they can influence SST, leading to the next warm event. Although SST variations exhibit weak westward propagation during some zonal mode events, POP analysis indicates that to first order there is no zonal propagation in SST. Net surface heat flux anomalies generally act to damp SST anomalies. The zonal mode explains a large amount (70%) of SST variability in the east and a sig-

nificant fraction (19%) of equatorial variability. Thus, the predictability potential in the Equatorial Atlantic on seasonal time scales may be considerably higher than currently thought.

3.1 Introduction

The zonal mode [*Xie and Carton*, 2004; *Zebiak*, 1993] dominates interannual climate variability in the Equatorial Atlantic. Zonal mode events primarily peak in boreal summer, but similar variability is also found in November-December [*Okumura and Xie*, 2006]. Associated SST anomalies can exceed 1°C in the Atlantic cold tongue (20°W and 0°W, 6°S and 2°N). Although much weaker than the El Niño Southern Oscillation (ENSO), the zonal mode has major socio-economic impacts, exerting a significant influence on surrounding countries [*Carton and Huang*, 1994], Indian-Summer monsoon [*Kucharski et al.*, 2008; *Wang et al.*, 2009], and possibly also ENSO [*Jansen et al.*, 2009; *Losada et al.*, 2009; *Wang*, 2006; *Wang et al.*, 2009].

The zonal mode's resemblance to ENSO suggests it may arise from similar coupled ocean-atmosphere interaction [*Zebiak*, 1993]. The Bjerknes positive feedback, involving equatorial zonal winds, SST, and upper ocean heat content (HC) is prominent in the structure of peak phase anomalies in observations and reanalysis [e.g., *Ruiz-Barradas et al.*, 2000]. However, each of its three elements explain less variance than in the Pacific [*Keenlyside and Latif*, 2007]. The existence of a delayed negative feedback – necessary for oscillatory behavior – has been investigated less [*Zebiak*, 1993; *Jansen et al.*, 2009]. Intermediate complexity models suggest that HC provides such a feedback and drives phase reversal [*Zebiak*, 1993], as in ENSO [*Jin*, 1997]. In these models, the zonal mode is a normal mode of coupled ocean-atmosphere dynamics [*Wang and Chang*, 2008]. Consistently, Atlantic equatorial averaged HC, from reanalysis and forced ocean model simulations, and observed cold tongue SST variations exhibit a quadrature relationship and are well fit by the recharge oscilla-

tor conceptual model [*Jansen et al.*, 2009]. However, despite similarities to ENSO, significant predictability of the zonal mode has not been shown.

The aim of this paper is to demonstrate that the zonal mode is an oscillatory normal mode of the observed coupled system, and that equatorial HC provides the delayed negative feedback for this mode, and hence a basis for seasonal prediction in the Equatorial Atlantic. We use both SSH and thermocline (20° isotherm) depth as proxies for upper ocean HC; all three quantities are closely related in the equatorial region, because of the two-layered nature of the tropical oceans. The paper is organized as follows. Section 3.2 gives a brief introduction to POP analysis and describes the data used. The oscillatory mechanisms of the equatorial Atlantic zonal mode are investigated in section 3.3 using primarily observations for the period 1993 to 2008. In section 3.4 these results are corroborated by repeating the analysis over a longer period (1958-2001) using data from an ocean model simulation. Conclusions and discussions are given in section 3.5.

3.2 Method and data

POP analysis [*Von Storch et al.*, 1988] is a linearized form of the more general Principal Interaction Pattern (PIP) analysis [*Hasselmann*, 1988] and used here to identify the normal modes of Equatorial Atlantic interannual climate variability. It is a method for extracting the eigenmodes of variability in multidimensional data. The POPs (or Empirical Normal Modes [*Penland and Sardeshmukh*, 1995]) are the eigenvectors of the system matrix A obtained by fitting the data to a multivariate first-order Markov process $\vec{X}(t+1) = A\vec{X}(t) + n$, where $A = C_1 C_0^{-1}$ with C_1 and C_0 denoting the lag +1 and lag 0 covariance matrices of $\vec{X}(t)$, and n a white noise forcing.

In general, POPs are complex with real and imaginary parts $\vec{P}^1$ and $\vec{P}^2$. They

can describe traveling modes or standing waves. The complex eigenvalues define a rotation period and an e-folding time for exponential decay. The time evolution $Z_1(t)$ and $Z_2(t)$ of the POPs are obtained from the projection of the original time series on the adjoint POPs. If the two coefficient time series are in quadrature, as theoretically expected, the evolution of the system in the two-dimensional POP space can be understand as a cyclic sequence of patterns: $\cdots \longrightarrow \vec{P}^2 \longrightarrow \vec{P}^1 \longrightarrow -\vec{P}^2 \longrightarrow -\vec{P}^1 \longrightarrow \cdots$.

After having identified a certain POP, it is often desirable to describe the signal in terms of other simultaneously observed variables $\vec{v}(t)$. Here, this is done with the "associated correlation pattern", denoted by $\vec{P}_v^1$ and $\vec{P}_v^2$. These can be obtained by minimizing $[\|\vec{v}(t) - \frac{Z_1(t)}{\sigma^1}\vec{P}_v^1 - \frac{Z_2(t)}{\sigma^2}\vec{P}_v^2\|]$. Here, $\|\|$ denotes a quadratic norm. The time coefficients $Z_1(t)$ and $Z_2(t)$ of the identified POP are normalized by their own standard deviation σ^1 and σ^2, respectively so that the patterns $\vec{P}_v^1$ and $\vec{P}_v^2$ have the same unit as variable $\vec{v}(t)$.

Here, two separate POP analysis are performed. The first covers the period 1993 to 2008 and uses satellite measurements of SSH (AVISO, http://www.aviso.oceanobs.com/) and SST (OISST, *Reynolds et al.* [2002]), and wind stress from the NCEP/NCAR reanalysis [*Kalnay et al.*, 1996]. The second covers the period 1958-2001 and uses observed reconstructed SST (HadISST, *Rayner et al.* [2003]), NCEP/NCAR reanalysis wind stress, and 20^{o}C isotherm depths from a NCEP/NCAR reanalysis forced ocean model [*Marsland et al.*, 2003] simulation. In the ocean model, standard bulk formulas for the calculation of heat fluxes and a weak relaxation of surface salinity to climatological observations [*Levitus and Boyer*, 1994] are used. Data from the simulation were used in previous studies of equatorial Atlantic variability [*Keenlyside and Latif*, 2007; *Jansen et al.*, 2009], where results were carefully checked using various other observations and reanalysis.

The domain analysed in this study is 45°W to 5°E and 10°S to 10°N, as we focus

on the equatorial zonal mode. However, our results are not sensitive to the exact choice of east-west domain (not shown). Prior to POP analysis, data were detrended and band-pass filtered to retain variations with periods between 8 and 80 months, and all quantities are normalized with their mean field standard deviation. The POP analysis uses the first six empirical orthogonal functions (EOFs), capturing 69.3% (68.1%) of the total variance for 1993-2008 (1958-2001) analysis. However, explained variance is always computed with respect to the raw monthly mean data. POP analysis using more than six EOFs reveals very similar results (not shown).

3.3 Results: 1993–2008

POP analysis of monthly SSH, SST, and wind stress reveals one dominant complex POP (Fig. 3.1a-d). It accounts for 19% of the total (unfiltered) variance, and considerably more locally: up to 40% in eastern Atlantic SSH (Fig. 3.2a), 70% in cold tongue SST (Fig. 3.2b), and 30% in South Atlantic surface zonal wind (Fig. 3.2c), but is low for meridional wind (Fig. 3.2d). This POP has a rotation period of 19 months, which is evident in the time evolution coefficients (Fig. 3.1e), and an e-folding time of 36 months. The period was corroborated by cross spectral analysis (not shown), which provides a robuster estimate [*Xu and Von Storch*, 1990]. It is shorter than other estimates from observations [30 months; *Latif and Grötzner*, 2000; *Ruiz-Barradas et al.*, 2000], theory [3 years; *Wang and Chang*, 2008], and intermediate complexity models [4 years; *Zebiak*, 1993]. This may reflect non-stationary behavior in the frequency of the zonal mode, given the different time intervals considered. All other POPs are not relevant to the zonal mode phenomenon.

The real POP component (Fig. 3.1b,d) is associated with the zonal mode's peak warm phase. It is consistent with the structure obtained from rotated-EOF analysis [*Ruiz-Barradas et al.*, 2000] and with an active Bjerknes feedback [*Keenlyside and Latif*, 2007]. SST anomalies in the eastern Equatorial Atlantic (Fig. 3.1d) are

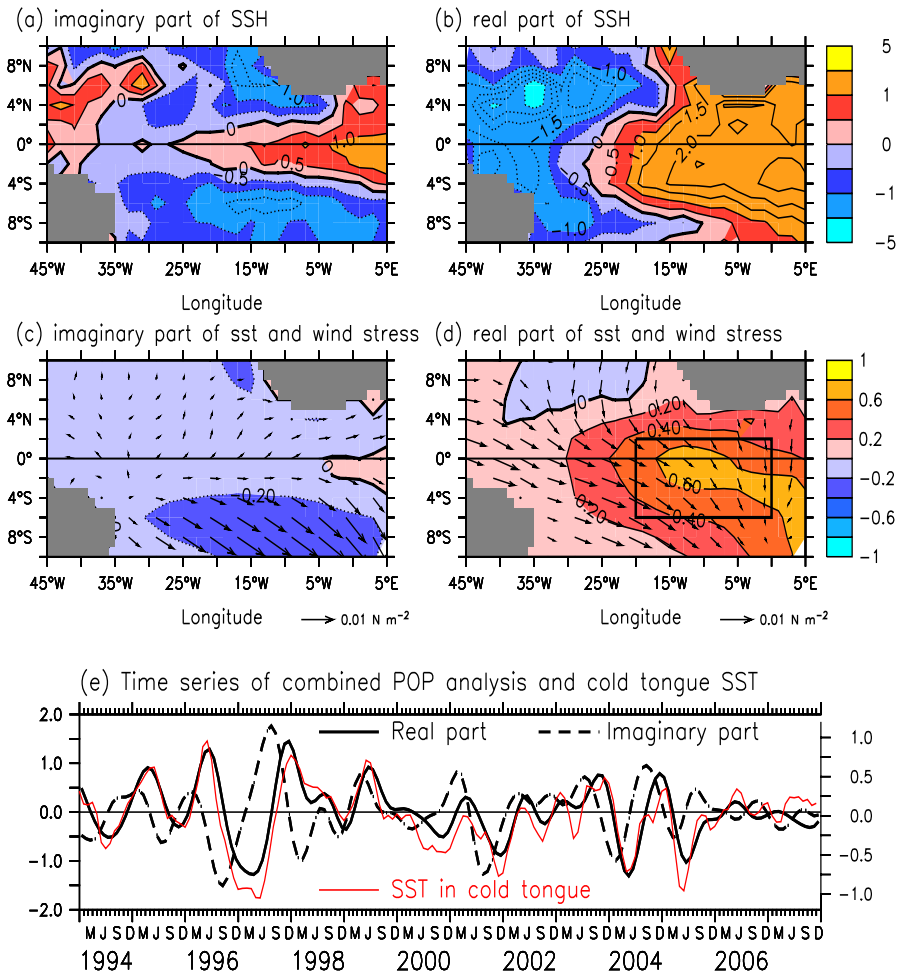

Figure 3.1: (a, b) SSH and (c, d) SST and wind stress from the dominant POP mode, (left) imaginary and (right) real components and (e) their corresponding time series and SST averaged over 20°W and 0°W, 6°S and 2°N (box in d). The maximum correlation between cold tongue SST and the real (imaginary) POP component time series is 0.89 (0.55) at zero-lag (when SST lags by 4-5 months). Real and imaginary components are most strongly related (r=0.7) when the imaginary component leads by 4-5 months.

accompanied by anomalous northwesterly surface winds to the west (Fig. 3.1d). Maximum negative SSH anomalies occur in the western Atlantic on both sides of the equator, while in the east there are strong positive anomalies at the equator; the pattern is reminiscent of Rossby and Kelvin wave structures. The imaginary POP component (Fig. 3.1a,c) corresponds to the transition phase, a quarter of the

rotation period prior to the peak. At this time a significant SSH signal has appeared in the equatorial wave guide (Fig. 3.1a), reflecting a build up of the HC. SST anomalies, however, are relatively weak (Fig. 3.1c) compared to those of the real component (Fig. 3.1d). Therefore, zonal mode SST variability can be regarded to first order as a standing oscillation (i.e., exhibiting no zonal propagation), although hovmoeller diagram of both raw and POP reconstructed SST anomalies (not shown) show weak westward propagation in some events. This is in contrast to *Wang and Chang* [2008], as SST anomalies in their theoretical mode migrate rapidly westward during the growth phase. In addition, in their mode SST variability extends to the northwestern Atlantic, while in our's it is constrained to the cold tongue. The zonal mode is argued to be a mixed SST-thermocline depth mode [*Zebiak*, 1993]. However, results here suggest the delayed-action/recharge oscillator mechanisms may dominate (consistent with *Jansen et al.* [2009]), given that heat content variations are important (Fig. 3.1a, b) and SST fluctuations exhibit a standing pattern (Fig. 3.1c, d).

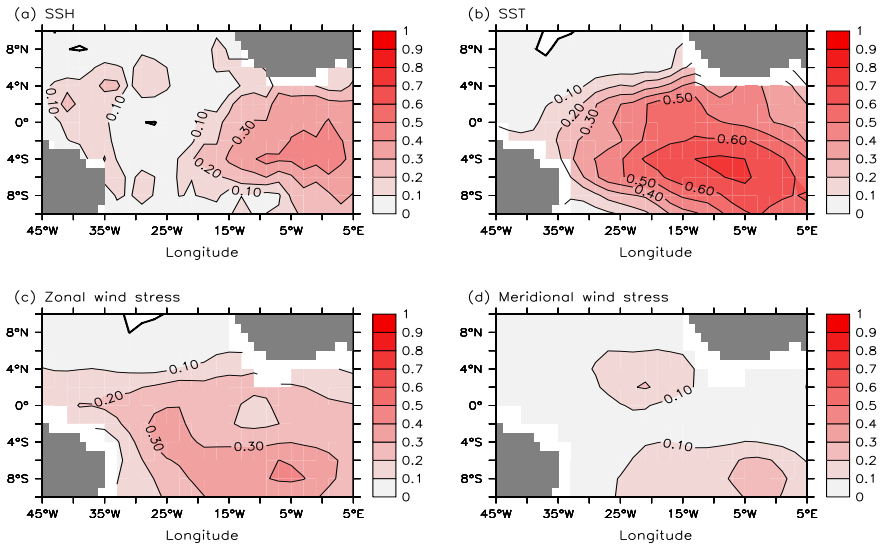

Figure 3.2: Local explained variances are computed using the dominant POP mode (Fig. 3.1) and with respect to raw monthly mean anomalies of (a) SSH, (b) SST, and (c) zonal and (d) meridional surface wind stress.

Interestingly, the POP mode also shows evidence of a northwesterly surface wind anomalies in the South Atlantic. These correspond to a relaxation of southeasterly Trades during the transition from the imaginary to real pop phases, and are consistent with development of warm anomalies there. Similar features are identified by composite and rotated-EOF analyses, which suggest an interaction among equatorial and Angola/Benguela SST variations and the South Atlantic anti-cyclone [*Hu and Huang*, 2007; *Lübbecke et al.*, accepted]. These studies indicate that the zonal mode is not a pure equatorial phenomenon, and that off-equatorial variations may be important in triggering the zonal mode.

The relevance of the recharge oscillator paradigm [*Jin*, 1997] in the Atlantic is further assessed by investigating the relationship between equatorial averaged HC (using SSH and thermocline depth as proxies) and cold tongue SST. SSH variations tend to lead SST variations, displaying a maximum correlation of 0.47 when SSH leads SST by about two months (Fig. 3.3). Data from the NCEP ocean reanalysis supports this relation, with equatorial averaged thermocline depth variations leading SST, with a maximum correlation (0.4) when thermocline depth variations lead by three months (Fig. 3.3). Different from SSH, thermocline depth and SST variations are in near quadrature with an almost zero simultaneous correlation. Forced ocean model simulations give similar results, with boreal summer equatorial averaged thermocline depth and autumn SST most strongly related [*Jansen et al.*, 2009]. The POP reconstruction exhibits a similar relationship, but it is stronger, and SSH and SST variations are less in quadrature (Fig. 3.3). It also indicates that equatorial averaged SSH acts as a delayed negative feedback for the zonal mode, as a strong anticorrelation (-0.6) occurs when SST variations lead SSH fluctuations by 6 months (Fig. 3.3). This phase relationship is in accord with model results [*Zebiak*, 1993] and the delayed action/recharge oscillator mechanism [*Jansen et al.*, 2009].

.

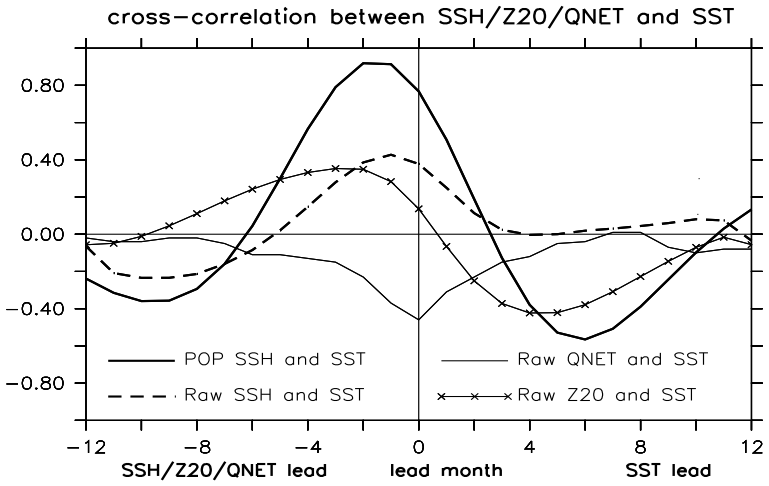

Figure 3.3: Cross-correlation between Equatorial Atlantic (3°S-3°N) averaged SSH and cold tongue averaged SST computed from the dominant POP mode, corresponding raw monthly mean data, and also using thermocline depth from NCEP reanalysis (http://www.esrl.noaa.gov/psd/) instead of SSH. Cross-correlation between cold tongue SST and net surface heat flux [*Yu and Weller*, 2007] is also shown. Period considered is 1993-2008.

It is useful to compare these results with those of the Pacific, where a similar relationship exists [*Meinen and McPhaden*, 2000]. There the maximum correlation (in raw data) is 0.77 when equatorial SSH anomalies lead Niño3 SST variations by 3 months (not shown). Thus, although upper ocean HC (as estimated by SSH and thermocline depth) provides memory for SST variability in the Atlantic on seasonal timescales, it is much less than in the Pacific. However, the relationship in the Atlantic might be underestimated in raw data, as fresh water perturbations to SSH in the west under the intertropical convergence zone may mask the dynamical signal and spoil the HC/SST quadrature relationship [*Schouten et al.*, 2005; *Ding et al.*, 2009]. The analysis of ocean model data below somewhat supports this notion.

The recharge/discharge of equatorial HC, achieved by equatorial waves, is evident in the vertical structure of equatorial upper ocean temperature during different phases of the zonal mode (Fig. 3.4). During the transition to the warm phase there is a build up of equatorial heat content, expressed in a basin wide deepening of the

thermocline that causes weak warm SST anomalies in the cold tongue (Fig. 3.4a). The positive Bjerknes feedback amplifies these anomalies and leads to the peak warm phase, with significant deepening of the thermocline in the east and strong SST anomalies at the surface (Fig. 3.4b). Discharge of equatorial HC has already begun at this time (Fig. 3.3), and cold subsurface temperature anomalies are intruding into the equatorial wave guide in the west (Fig. 3.4b). The latter accumulate and propagate eastward causing basin wide negative anomalies in the thermocline (i.e., the negative of Fig. 3.4a), which in turn lead to cooling in the cold tongue and the negative phase of the zonal mode. These subsurface temperature changes are reminiscent of those in the Pacific, providing further support for the delayed action/recharge oscillator mechanism in the Atlantic.

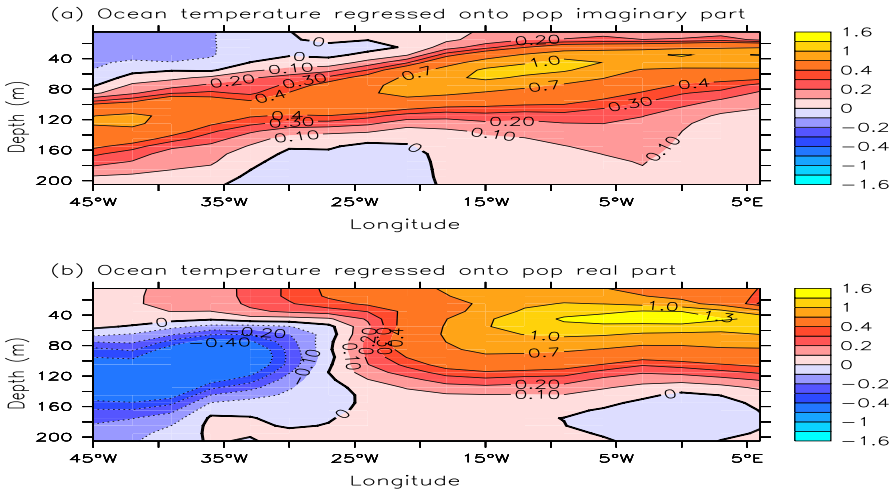

Figure 3.4: Associated correlation pattern in subsurface temperature anomalies along the equator during the (a) transition and (b) peak phases of the zonal mode, as respectively obtained by linear regression of imaginary and real POP time coefficients (Fig. 3.1) on to NCEP reanalysis ocean temperature.

Analysis above indicates that interannual variability in Equatorial Atlantic SST results mainly from ocean dynamics. This is supported by the simultaneous anti-correlation (-0.46) between net surface heat flux and SST averaged over the cold tongue (Fig. 3.3); this is consistent with previous studies that found that surface

heat flux variations damp SST anomalies in the eastern South Atlantic near the Gulf of Guinea [*Hu and Huang*, 2006; 2007]. Although net surface heat flux mainly damps SST variability, it can sometimes help drive SST changes, for example following strong El Niño events [*Chang et al.*, 2006] and in the western tropical Atlantic [*Hu and Huang*, 2006; 2007]; surface heat flux variations may also be important in driving SST anomalies on shorter time scales. The complexity of the upper ocean heat budget adds difficulty to seasonal prediction of Equatorial Atlantic variability [*Chang et al.*, 2006].

3.4 Results: 1958–2001

The POP analysis of SST, 20^oC isotherm depth, and surface wind stress for the period 1958-2001 reveals one dominant complex POP (Fig. 3.5), accounting for 20% of the total (unfiltered) variance. This POP has a rotation period of 30 months (confirmed by cross spectral analysis) and an e-folding time of 26 months. The period is longer than that found above, but consistent with other estimates from observations [30 months; *Latif and Grötzner*, 2000; *Ruiz-Barradas et al.*, 2000]. No other POPs are relevant here.

The POP patterns (Fig. 3.5) bear strong resemblance to those obtained from data for the shorter period (Fig. 3.1), with one main difference: during the transition phase heat content anomalies of same sign extend along the whole of the equator (Fig. 3.5a); this is more consistent with the delayed-action/recharge oscillator mechanisms. Another difference is that compared to Fig. 3.1d, the SST anomaly pattern in Fig. 3.5d is less focused on the equator and may have a stronger projection onto the meridional mode [*Ruiz-Barradas et al.*, 2000; *Wang and Chang*, 2008]. Local explained variances (Fig. 3.6a) in thermocline depth also display a more consistent structure with equatorial Rossby and Kelvin waves than in SSH (Fig. 3.2a). This is consistent with fresh water perturbations masking the dynamical

signal in sea level under the ITCZ in the western tropical Atlantic [*Schouten et al.*, 2005; *Ding et al.*, 2009]. Correlation between simulated thermocline depth and observed SSH from 1993 to 2001 (not shown) is low (0.2) in those areas where explained variances in SSH is low (less than 10%) but higher (over 0.4) in regions of high explained variance in SSH. Local explained variances in SST, zonal and meridional wind stress display some difference, possibly due to the different time interval analyzed. These data also support the relationship between equatorial heat content and cold tongue SST (Fig. 3.7), but it is somewhat weaker than in the SSH and SST above (Fig. 3.3) (possible reasons for this are described in the next section). The subsurface temperature patterns during transition and mature phase are also very similar to those above (not shown). These results therefore support the mechanisms presented by POP analysis of relatively short data.

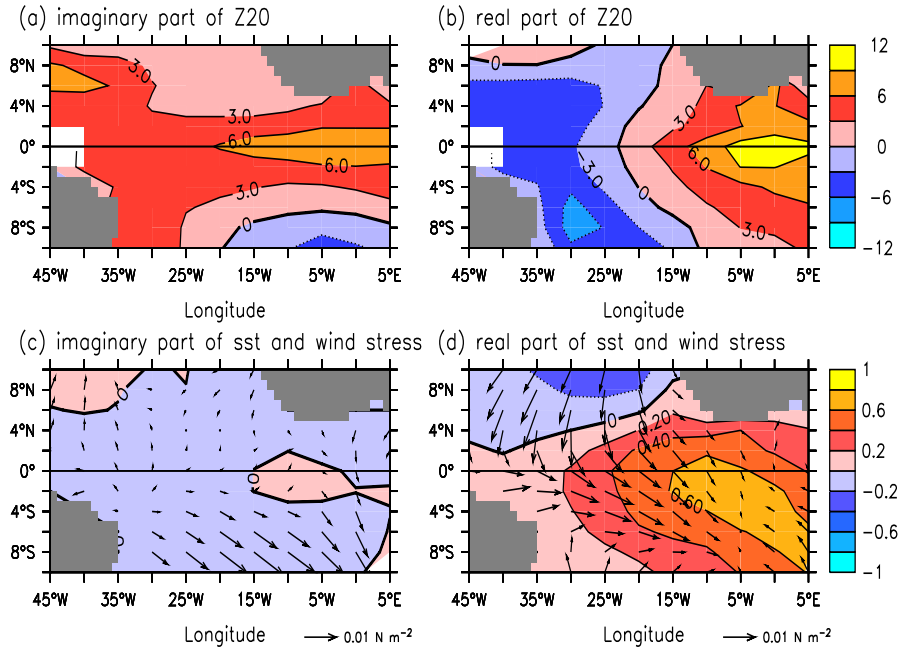

Figure 3.5: (a, b) 20^{o}C isotherm depth (Z20) and (c, d) SST and wind stress from the dominant POP mode, (left) imaginary and (right) real components. This figure corresponds to Fig. 3.1, but 20^{o}C isotherm depth from a forced ocean model simulation are used instead of SSH, and the period 1958-2001 is considered.

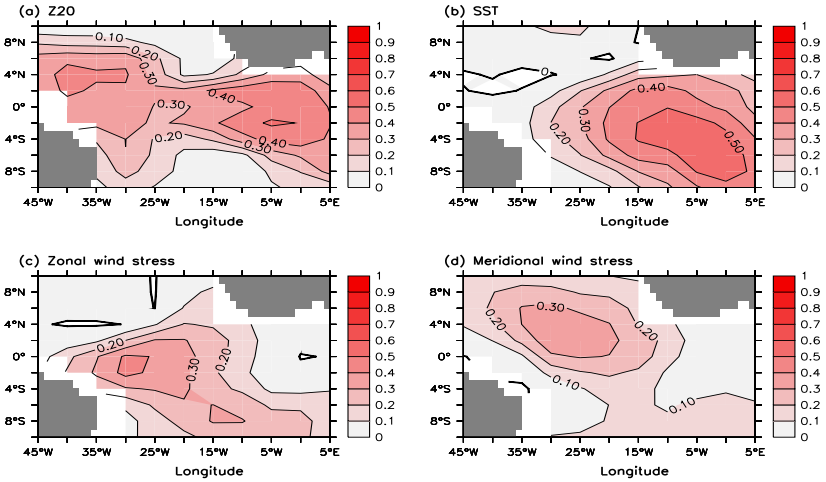

Figure 3.6: Local explained variances are computed using the dominant POP mode (Fig. 3.5) and with respect to raw monthly mean anomalies of (a) 20^{o}C isotherm depth (Z20), (b) SST, and (c) zonal and (d) meridional surface wind stress. This figure corresponds to Fig. 3.2, but 20^{o}C isotherm depth from a forced ocean model simulation are used instead of SSH, and the period 1958-2001 is considered.

3.5 Conclusions and discussion

The zonal mode is identified as a normal mode of observed Equatorial Atlantic interannual variability, through POP analysis of essentially observational data between 1993-2008. During this interval, it explains 19% of the total variance and has a period of 19 months. The zonal mode is dominated by delayed action/recharge oscillator mechanism, where HC (as measured by SSH and thermocline depth) provides memory, and thus a basis for seasonal prediction. This work supports previous studies based on intermediate complexity [*Zebiak*, 1993], and conceptual models [*Jansen et al.*, 2009], and provides further evidence for the role of HC in Equatorial Atlantic variability. POP analysis of longer data sets (1958-2001) corroborates the mechanism proposed here, despite identifying a different oscillation period (30 months). Previous studies (e.g., *Zebiak* [1993]; *Frankignoul and Kestenare* [2005]; *Illig and Dewitte* [2006]; *Wang and Chang* [2008]) indicate that the zonal mode is stable, and that external/stochastic forcing is required to sustain it. The oscillatory charac-

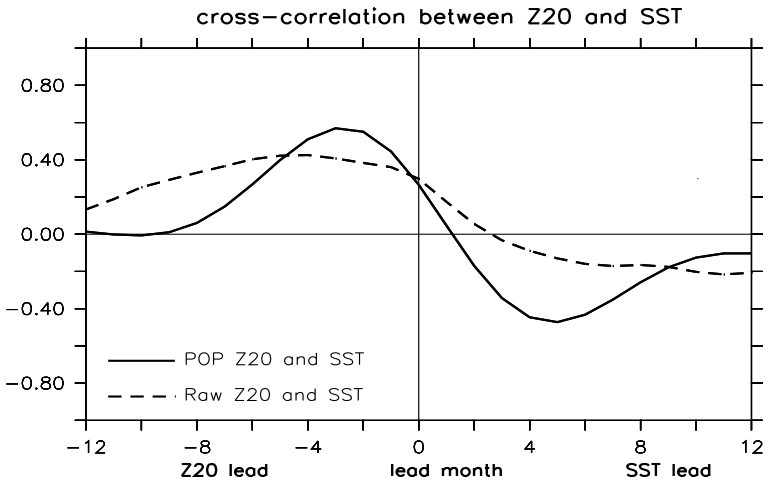

Figure 3.7: Cross-correlation between Equatorial Atlantic (3°S-3°N) averaged 20^{o}C isotherm depth (Z20) and cold tongue averaged SST computed from the dominant POP mode and corresponding raw monthly mean data. This figure corresponds to Fig. 3.3, but 20^{o}C isotherm depth from a forced ocean model simulation are used instead of SSH, and the period 1958-2001 is considered.

ter revealed by POP method does not contradict these studies. Furthermore, POP analysis cannot directly address the stability of the zonal mode, as it is a linear analysis.

The shorter period found in the analysis of data from 1993 to 2008 may reflect non-stationarity in the frequency of zonal mode, but it could also be due to the short length of data. POP analysis of the sub-periods 1956-1970, 1971-1985 and 1986-2000 identifies dominant periods of 28, 23 and 22 months, respectively. Although this is consistent with non-stationarity, sensitivity to data length cannot be completely excluded, as all three periods are shorter than 30 months. The literature also reports quite different estimates for the dominant period of the zonal mode (e.g., 30 months [*Latif and Grötzner*, 2000; *Ruiz-Barradas et al.*, 2000], 4 years [*Zebiak*, 1993; *Jansen et al.*, 2009]), but all are longer than 19-months. Estimated periods are generally not equal to an integral number years, despite the strong seasonality of the zonal mode [*Xie and Carton*, 2004]. Thus, the interaction with the annual cycle is a further

complication in estimating the zonal mode's period. Longer high-quality data are required to resolve these issues.

The variance explained by the zonal mode is locally large and up to 70% in cold tongue SST (Fig. 3.2b). Given the importance of this mode for precipitation in surrounding countries, it is important to be able to predict it to the extent possible. The level of predictability may be estimated from the oscillatory nature of the POP. The maximum lagged-linear correlation between the imaginary component time series and cold tongue SST (r=0.55; Fig. 3.1e) suggests around 30% (r=0.55) of cold tongue SST variability could be predicted at 4-months lead. And around 80% (r=0.9) at 2-months lead, implied by the relationship with equatorial averaged heat content POP (Fig. 3.3). These values are consistent with estimates based on fitted conceptual models [*Jansen et al.*, 2009]. Nevertheless they are based on a highly simplified picture and higher values may be achievable using complex dynamical models, and in particular seasons and for specific events [*Kleeman and Moore*, 1999].

The direct relationship between equatorial averaged SSH and cold tongue SST (Fig. 3.3) implies much lower skill, reflecting that equatorial averaged SSH and the imaginary POP are poorly related (Fig. 3.1a). This may be because SSH is not an ideal proxy for HC, as in the NCEP ocean reanalysis (not shown) and forced ocean model simulations (Fig. 3.5), equatorial averaged thermocline depth and the imaginary POP are closely related. However, the relationship between equatorial heat content and cold tongue SST remains weak in these products (Fig. 3.3 & 3.7). But differences among these products are not small, due to model deficiencies, sparse ocean data for assimilating, and inaccurate surface forcing.

Alternatively, the recharge oscillator mechanisms may explain much less variance than suggested by the POP analysis or other dynamics may better describe equatorial Atlantic variability. In particular, complex remote forcing from ENSO [*Chang et al.*, 2006] might contribute to mask the HC signal. Also, unlike in the Pacific, the

Atlantic equatorial cold tongue is centered south of the equator and how equatorial waves influence this region may be different. Other possible mechanisms include, the western Pacific oscillator [*Weisberg and Wang*, 1997], advective-reflective oscillator [*Picaut et al.*, 1997; *Wang*, 2001], or a destabilized basin mode [*Jin and Neelin*, 1993; *Keenlyside et al.*, 2007]. The western Pacific oscillator, however, is probably not active in the Atlantic, as no negative SST or westward wind stress anomalies exist in the western Atlantic during the zonal mode's peak phase (Fig 3.1b). Zonal current variations are important in both the advective-reflective oscillator and destabilized basin-mode mechanisms. Preliminary analysis of zonal currents, model and satellite-derived, suggest a possible role for the basin mode (not shown). However, explained variances are substantially smaller than that for heat content (SSH and thermocline depth). Further analysis and better ocean heat content data are required to resolve these issues.

Results here offer some promise for seasonal prediction in the Atlantic. However, two things are required before useful skill might be realised. First, the major systematic errors of complex models [*Davey et al.*, 2002; *Richter and Xie*, 2008; *Wahl et al.*, 2009] in simulating the equatorial Atlantic climate need to be reduced. In most models these errors are so large that they inhibit feedbacks necessary for interannual variability. Second, better observations of upper ocean heat content in the Equatorial Atlantic are required to accurately initialised forecasts. We hope that this work should further stimulate developments in these two areas.

Acknowledgments

The work was supported by the German BMBF NORDATLANTIK project and the SFB 754 of DFG. POP calculations were performed at the Rechenzentrum der Univerität Kiel. NSK is funded by the DFG Emmy Noether Programme. Fig-

ures were created using Ferret, a product of NOAA's Pacific Marine Environmental Laboratory.

Chapter 4

Impact of the Equatorial Atlantic on the El Niño Southern Oscillation

Abstract

The influence of Atlantic zonal mode on the El Niño Southern Oscillation (ENSO) in the Pacific is investigated in observations and reanalysis and with coupled model simulations. Observations show that the warm (cold) phase of the Atlantic zonal mode during boreal summer favours the development of La Niña (El Niño) during boreal winter. Warm sea surface temperature (SST) anomalies associated with the Atlantic zonal mode affect the Walker Circulation with anomalous high sea level pressure and descending motion over the eastern Tropical Pacific. The anomalous high pressure drives westward wind anomalies that increase the east-west thermocline slope, with shallowing and deepening in the eastern and western Pacific, respectively. The shallower thermocline causes cooling of SST in the east, enchancing the surface easterlies. In the following autumn and winter, these anomalies in wind, thermocline and SST are amplified further by the Bjerknes positive feedback, favouring the development of a La Niña event. The same mechanisms act for the cold phase of Atlantic zonal mode, but with opposite sign. Experiments with the ECHAM5/MPIOM coupled

general circulation model (CGCM) for the period 1950-2005 support this mechanism. Five ensemble member simulations forced with observed SST in the Tropical Atlantic, but with full air-sea coupling allowed in the Pacific and Indian, reproduce the observed results very well.

4.1 Introduction

In the tropical Pacific, the El Niño Southern Oscillation is the dominant mode of interannual climate variability. It results from ocean-atmosphere interaction [*Bjerknes*, 1969; *Philander*, 1990]. ENSO events often begin in boreal spring and summer and reach their peak in boreal winter. The changes in the atmospheric circulation caused by ENSO affect weather around the world [e.g., *Glantz et al.*, 1991], having large economic and social impacts. In the equatorial Atlantic, the dominant mode of interannual variability results from similar ocean-atmosphere interaction [*Zebiak*, 1993; *Xie and Carton*, 2004; *Keenlyside and Latif*, 2007; *Jansen et al.*, 2009; *Ding et al.*, 2010], and is termed the "Atlantic zonal mode" or "Atlantic Niño". However in the Atlantic, the variability has different seasonality, and anomalous events in sea surface temperature (SST) often reach their mature phase during boreal summer [*Keenlyside and Latif*, 2007].

Recent studies have suggested that Atlantic zonal mode variability might influence ENSO [e.g., *Wang*, 2006; *Keenlyside and Latif*, 2007; *Jansen et al.*, 2009; *Rodríguez-Fonseca et al.*, 2009; *Losada et al.*, 2009]. *Wang* [2006] found that Tropical Atlantic and Pacific SST anomalies form an inter-basin gradient and positive feedback with overlying Walker Circulation, indicating an interaction between the two tropical ocean basins. Whereas, *Keenlyside and Latif* [2007] indicate there is a significant correlation between Atlantic and Pacific Niños, when the Atlantic leads by six-months. *Jansen et al.* [2009] showed that a feedback from the Atlantic on ENSO appears to exist, which slightly improves the retrospective forecast skill in

a conceptual recharge oscillator model [*Burgers et al.*, 2005]. *Losada et al.* [2009] studied the tropical response to the Tropical Atlantic SST anomalies using four atmospheric general circulation models (AGCMs). Their results show that the SST anomalies produce a Gill-type response, which extends into eastern Tropical Pacific. *Rodríguez-Fonseca et al.* [2009] investigated the tropical Atlantic influence on ENSO events from a coupled perspective. Analysing observation and reanalysis, they showed that Atlantic zonal modes are associated with surface wind anomalies in the summer in the Equatorial Pacific. They argued that these are subsequently amplified by the Bjerknes positive feedback, causing an ENSO event peaking in the boreal winter. Thus, explaining the significant correlation when Atlantic variability leads that in the Pacific by six-months [*Keenlyside and Latif*, 2007]. To support the mechanisms they performed ensemble simulations with a coupled model (an AGCM coupled to 1.5 layer ocean model) with observed SST prescribed in the Atlantic, but fully coupled elsewhere. However, their model results are not entirely consistent with observations. Specifically, the observed consistent signal among wind stress, thermocline depth and sea surface temperature from the boreal summer to winter was not well reproduced. Thus, it is worthwhile to re-investigate the mechanism for the influence of the Tropical Atlantic on ENSO.

Several recent studies show that the Atlantic zonal mode may also influence the Indian Monsoon [*Kucharski et al.*, 2007; 2008; 2009; *Losada et al.*, 2009]. Using an AGCM coupled to the MICOM ocean model in the Indian Ocean, *Kucharski et al.* [2007] argued that the Atlantic zonal mode variability regulates the relationship between Indian Monsoon Rainfall and ENSO. *Losada et al.* [2009] investigated atmospheric response to SST anomalies associated with Atlantic zonal mode using four AGCMs. Their model results show that the atmospheric response extends into the Indian Ocean. However, as discussed above, the Atlantic zonal modes may affect ENSO and thus indirectly the Indian Ocean [*Klein et al.*, 1999; *Xie et al.*, 2002; *Krishnamurthy and Kirtman*, 2006]. What is the net influence if we consider both

direct and indirect effects on Indian Ocean? A model coupled over the Tropical Pacific and Indian Oceans is required to answer this question and to study the Tropical Atlantics influence on the Indian Monsoon.

In this study, we employ observations, reanalysis, and a fully coupled climate model (ECHAM5/MPI-OM) to address the questions presented above. In section 2, we give a brief introduction to the model employed in this study and the experimental design. In section 3, we investigate the Atlantic zonal modes influence on the Pacific using observations and reanalysis. In section 4 the mechanisms identified, as hypothesised already by *Rodríguez-Fonseca et al.* [2009], is confirmed by analysing the coupled model experiments. Discussion and conclusions are given in section 5.

4.2 Data, Model and experimental setups

Sea surface temperature data are taken from the Hadley Center Sea Ice and Sea Surface Temperature dataset version 1.1 (HadISST 1.1), which is an EOF-based reconstruction of observations extending from the present until 1870 [*Rayner et al.*, 2003], and are provided by the British Atmospheric Data Center (http://badc.nerc.ac.uk/home/). Sea level pressure (SLP) and wind stress are taken from NCEP/NCAR reanalysis [*Kalnay et al.*, 1996]. Stream function and velocity potential are calculated from NCEP/NCAR zonal and meridional wind components [*Kalnay et al.*, 1996]. CMAP satellite derived precipitation data [*Xie and Arkin*, 1997] are available from 1979 up to present, provided by the NOAA/OAR/ESRL PSD, Boulder, Colorado, USA (http://www.esrl.noaa.gov/psd/). Thermocline depth data is calculated from NCEP ocean temperature reanalysis, which is available from 1980 to present.

In this study, the Max-Planck-Institute (MPI) coupled model ECHAM5/MPI-OM (IPCC version) is employed. The atmosphere model (ECHAM5) is run at T63 spectral resolution (1.875x1.875) with 31 vertical (hybrid) levels. The ocean (MPI-

OM) has 1.5 degree average horizontal grid spacing with 40 unevenly spaced vertical levels. Atmosphere and ocean are coupled by means of the Ocean-Atmosphere-Sea Ice-Soil (OASIS) coupler [*Valcke et al.*, 2003]. The model does not require flux adjustment to maintain a stable climate, and simulates the mean state, and annual and interannual variability in the Tropical Pacific well: Mean deviations from observed sea surface temperature is less than 1 K over much of the Tropical Pacific, and the phase and strength of the simulated annual cycle of SST in the equatorial Pacific match observations [*Jungclaus et al.*, 2006]. The simulated ENSO has a dominant period of around 4 year, and its spatial pattern is in agreement with observations. The model was used to study seasonal-to-decadal prediction and predictability in the ENSEMBLES project [*Keenlyside et al.*, 2008].

Here a partial coupled configuration of the model is used, with full coupling everywhere except in the Atlantic, where model SSTs are nudged to observations: between 30°S and 30°N the damping constant equals 0.25d ($3.8 \times 10^3 Wm^{-1}K^{-1}$); poleward of these latitudes the damping constant decreases linearly to zero at 60°S and 60°N. Here, full observed SST is nudged into the model. SST anomalies are not used because the model exhibits a warm SST bias in the Tropical Atlantic, a feature common to most CGCMs [*Davey et al.*, 2002; *Richter and Xie*, 2008; *Wahl et al.*, 2009]. National Center for Environmental Prediction (NCEP) reanalysis [*Kalnay et al.*, 1996] skin temperature (obtained from the Climate Diagnostics Center; see http.//www.cdc.noaa.gov) is used for the observed SST. The model is run from 1950 to 2005 with five ensemble members, differing in the initial conditions. Prior to 2000, radiative forcing is computed from observed changes in greenhouse gas concentrations, sulphate aerosol loadings, and the solar cycle, and accounts for major volcanic eruptions; after 2000 it follows the IPCC A1B scenario. The ensemble mean of these simulations is analyzed. It reduces the contribution of internal dynamics in the Indo-Pacific sector by a approximately 0.45, while retaining the influence from the Tropical Atlantic.

4.3 Atlantic zonal mode's influences on ENSO in observation and reanalysis

The observed relation between Atlantic zonal mode and ENSO events was stronger since 1960s [*Kozlenko et al.*, 2009; *Rodríguez-Fonseca et al.*, 2009], and thus the period since 1970 is only considered here, unless otherwise mentioned.

The observed cross correlation between Niño3 (150°W-90°W, 5°S-5°N) SST and Atlantic cold tongue (20°W-0°W, 6°S-2°N) SST shows that no significant relation exists at zero lag or when Pacific variability leads (Fig. 4.1a). This indicates that ENSO has no significant (linear) influence on Atlantic zonal mode, consistent with previous studies [*Enfield and Mayer*, 1997; *Chang et al.*, 2006]. In contrast, when the Atlantic cold tongue index leads Niño3 SST variations by about six months, there is a significant maximum anti-correlation of -0.42 (Fig. 4.1a) [*Keenlyside and Latif*, 2007]. This indicates that warm (cold) SST anomalies associated with Atlantic zonal mode events may strengthen the negative (positive) phase of ENSO six months later. The lag of six months possibly comes from the different seasonality of Atlantic and Pacific interannual variability: Previous studies showed that the Atlantic zonal mode events often reach their mature phase during boreal summer [*Carton and Huang*, 1994; *Keenlyside and Latif*, 2007], while ENSO events peak during boreal winter [*Philander*, 1990].

How does Atlantic zonal mode influence ENSO? Warm (cold) SST anomalies in the equatorial Atlantic can influence the overlying Walker Circulation, producing low (high) and high (low) SLP anomalies in the Atlantic and eastern Pacific *Wang* [2006]. The high (low) SLP anomalies in the Pacific induce easterly (westerly) wind stress anomalies over the western and central Tropical Pacific. Consistently, Atlantic cold tongue SST anomalies display a significant anti-correlation (Fig. 4.1b) with zonal wind stress anomalies averaged from western to central equatorial Pacific (140°E-170°W, 5°S-5°N) from March to August. The zonal wind stress anomalies in

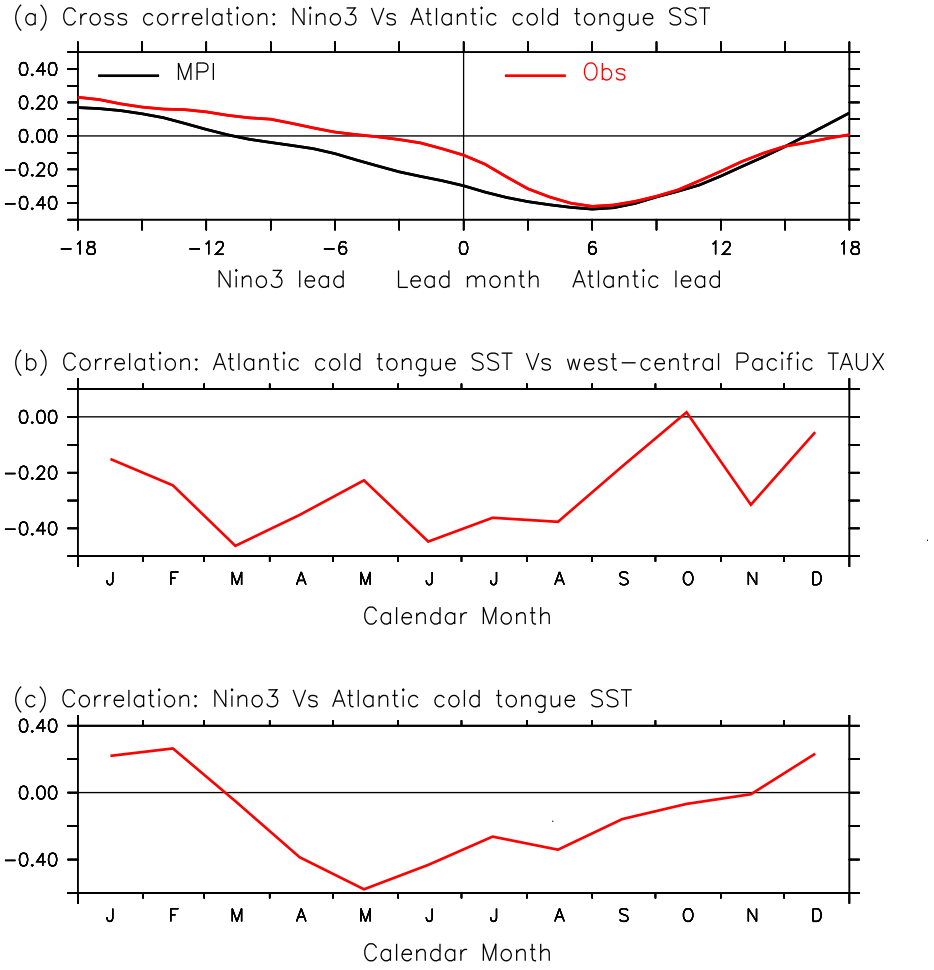

Figure 4.1: (a) Cross correlation between Niño3 and Atlantic cold tongue SST for HadISST (red) and the ensemble mean of the MPI model simulations with observed SST prescribed in the Atlantic (black). (b) Monthly stratified correlation between Atlantic cold tongue SST (HadISST) and zonal wind stress (NCEP) averaged in the western to central equatorial Pacific (140°E-170°W, 5°S-5°N). (c) Monthly stratified correlation between Niño3 and Atlantic cold tongue SST (HadISST).

this region are critical for Bjerknes positive feedback of ENSO [*Jin*, 1997]. During this time, an ENSO event is in its onset phase and anomalies are weak [*Philander*, 1990]. Therefore, it is possible for the signal from the Atlantic zonal mode to influence the Bjerknes positive feedback loop of ENSO and the following evolution of the ENSO event. Conistently, Atlantic cold tongue and Niño3 SST anomalies

show a significant negative correlation from the April to August (Fig. 4.1c). In the following, we will expand on this mechanism.

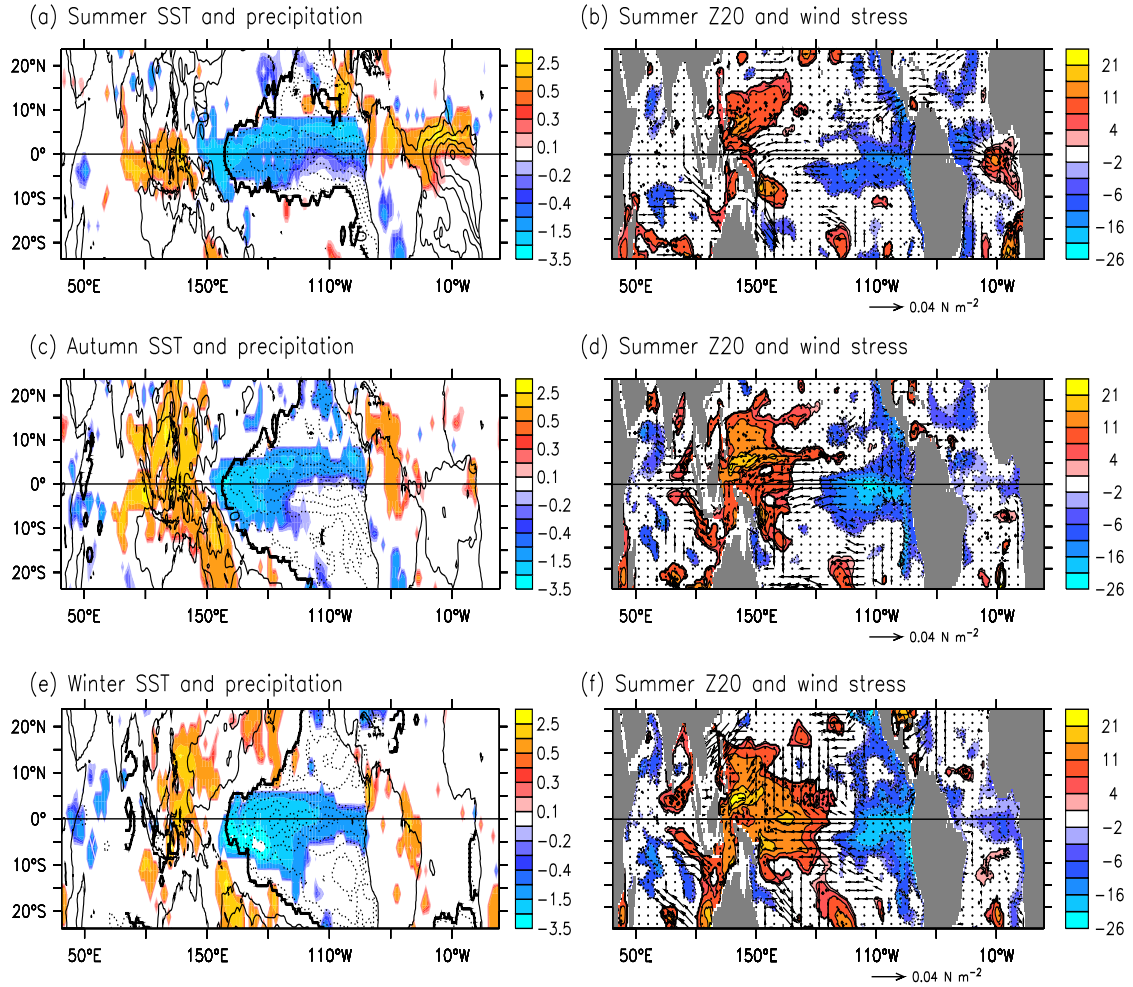

Figure 4.2: (a, c and e) Sea surface temperature (contour, HadISST) and precipitation (shading, *Xie and Arkin* [1997]), and (b, d and f) thermocline depth (shading, NCEP reanalysis) and wind stress (vector, *Kalnay et al.* [1996]) in boreal summer (a, b), autumn (c, d) and winter (e, f) regressed onto boreal summer Atlantic cold tongue SST. The units for precipitation, thermocline depth and wind stress are $mm\ day^{-1}$, m and Nm^{-2}, respectively. The contour interval of SST is $0.2°C$ with positive and negative values shown with solid and dashed curves, respectively. Only those values which are over 95% statistically significant under a Student t-test are shown.

Warm SST anomalies of an Atlantic zonal mode occur along with a southward

shift of tropical convection [*Wagner and Da Silva*, 1994; *Carton et al.*, 1996] and more precipitation in the equatorial Atlantic region during boreal summer (Fig. 4.2a). The positive precipitation anomalies cause diabatic heating of the atmosphere, warming up the whole troposphere and influencing atmospheric circulation [*Ruiz-Barradas et al.*, 2000]. The corresponding stream function and velocity potential anomalies at the 200 hPa in boreal summer show a pair of anti-cyclones both sides of the equator and divergent motion over the Tropical Atlantic (Fig. 4.3a). The anomalies extend to the Tropical Pacific, with convergent motion there. The pattern at 200hPa is consistent with AGCM studies *Losada et al.* [2009], indicating these anomalies are indeed driven by Atlantic SST anomalies. Corresponding with these anomalies, there are low (ascending) and high (descending) SLP (vertical velocity) anomalies (Fig. 4.3b) over the Atlantic and eastern Pacific (Fig. 4.3a), respectively. The anomalous high pressure and descending motion over the Pacific suppresses convective activity and reduces precipitation there (Fig. 4.2a). These results suggest that the Atlantic zonal mode influences the atmospheric circulation in the Tropical Pacific via the Walker Circulation, consistent with previous studies *Wang* [2006].

High sea level pressure anomalies (Fig. 4.3b) in the Tropical Pacific would produce easterly wind stress anomalies over the western and central Tropical Pacific (Fig. 4.2b). Zonal wind anomalies over this region are a very important component in the Bjerknes positive feedback. The wind stress anomalies associated with an Atlantic zonal mode event (Fig. 4.2a) would increase the east-west gradient in the thermocline, causing shallowing (deepening) in the east (west) (Fig. 4.2b). A shallower thermocline in the east (Fig. 4.2b) means colder subsurface water is advected upward into mixed layer, reducing sea surface temperature (Fig. 4.2a). The reduced SST would enhance the easterly wind stress anomalies, forming a Bjerknes positive feedback loop. Therefore, the Atlantic zonal modes is associated with wind stress, thermocline depth and SST anomalies consistent with the Bjerknes positive feedback. In the following autumn and winter, the Atlantic zonal mode dies away

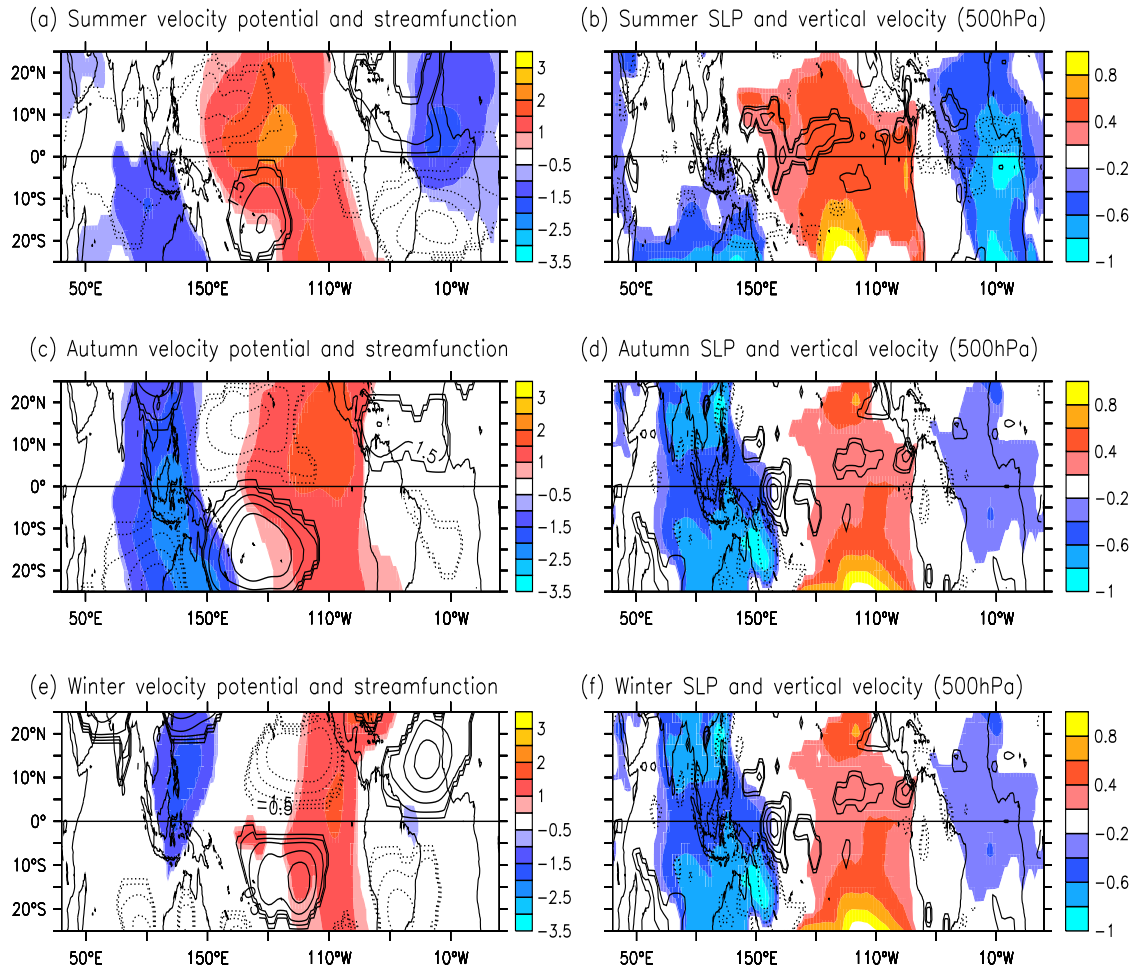

Figure 4.3: (a, c and e) Stream function (contour) and velocity potential (shading) and (b, d and f) sea level pressure (shading) and vertical velocity (contour) at the 500hPa in boreal summer (a, b), autumn (c, d) and winter (e, f) regressed onto boreal summer Atlantic cold tongue SST (HadISST). Atmospheric data are from NCEP/NCAR reanalysis [*Kalnay et al.*, 1996]. The units for velocity potential and sea level pressure are $10^6 m^2 s^{-1}$ and hPa, respectively. The contours shown for stream function (vertical velocity) are $\pm 4.5, \pm 3.5, \pm 2.5, \pm 1.5$ $and \pm 0.5 \times 10^6 m^2 s^{-1}$ ($\pm 2.5, \pm 2.0, \pm 1.5, \pm 1.0, \pm 0.5$ $and \pm 0.25 \times 10^{-2} Pas^{-1}$). Positive and negative values are shown by solid and dashed contours, respectively. Note that negative vertical velocity mean upward motions. Only those values which are over 95% statistically significant under a Student t-test are shown.

and has little influence on the atmospheric circulation (Fig. 4.2 and 4.3 b, c), but the Bjerknes feedback still acts enhancing SST, the east-west thermocline gradient

and easterly wind stress anomalies in the Pacific (Fig. 4.2b, c). The mechanism revealed here is consistent with previous studies [*Rodríguez-Fonseca et al.*, 2009].

4.4 Atlantic zonal mode's influences on ENSO in CGCM

So far, we have investigated the Atlantic zonal mode influence on ENSO events and corresponding mechanisms in terms of observations and reanalysis. However, observations offer only one realization and the relationship between Atlantic zonal mode and ENSO could be fortuitous. To confirm the relationship revealed by observations and reanalysis, we employ a full CGCM and perform a set of experiments in which observed SST are prescribed in the Atlantic (See section 4.2 for details). In this study, the ensemble mean of the five model runs is analyzed. The cross correlation between Atlantic cold tongue and Niño3 SST anomalies simulated by the model matches the observed one very well (Fig. 4.1a). In particular, the model reproduces the maximum anti-correlation when the Atlantic cold tongue index leads Niño3 SST by about six months. This indicates that corresponding to prescribed warm (cold) SST anomalies associated with the Atlantic zonal mode, the model displays strengthened cold (warm) phase of ENSO. There exist some discrepancies between observations and the model. For instance, model displays a simultaneous anti-correlation of -0.3, while observations displays no simultaneous relationship. This discrepancy is not surprising given ensemble mean is performed. The good agreement between observations and the model simulations provides confidence to use the model to investigate the mechanisms connecting variability in the two basins.

Associated with warm SST anomalies (Fig. 4.4a) of the Atlantic zonal mode in boreal summer, there are positive precipitation anomalies (Fig. 4.4a) in the equatorial Atlantic region. The corresponding diabatic heating produces a pair of anti-cyclone and divergent motion over the Tropical Atlantic at 200hPa (Fig. 4.5a).

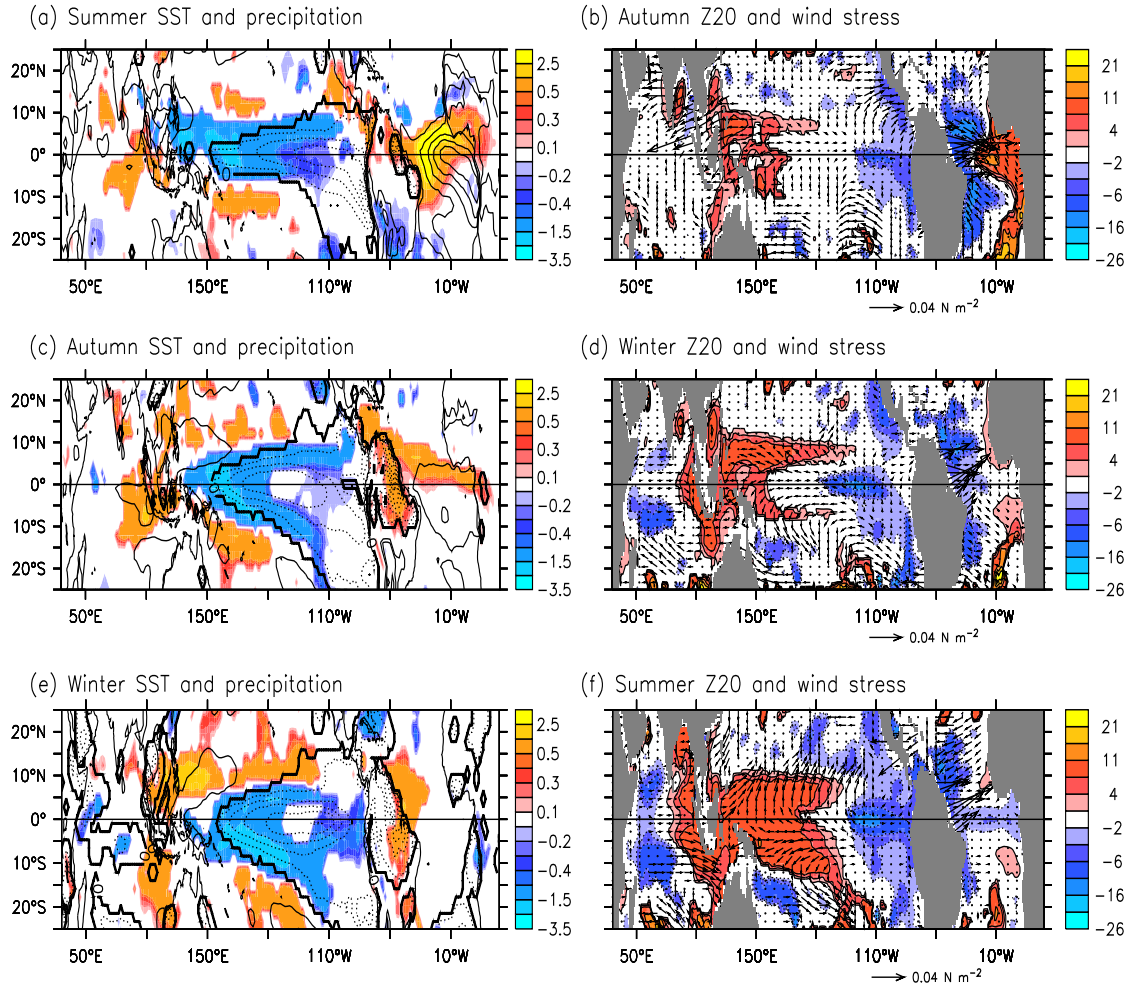

Figure 4.4: (a, c and e) Streamfunction (contour) and velocity potential (shading) and (b, d and f) sea level pressure (shading) and vertical velocity (contour) at the 500hPa in boreal summer (a, b), autumn (c, d) and winter (e, f) regressed onto boreal summer Atlantic cold tongue SST. All of the quantities are from ensemble mean of five model runs. The shading and contours are the same as in Fig. 4.2. Only those values which are over 95% statistically significant under a Student t-test are shown.

The atmospheric response at this level also extends into the tropical Pacific with a pair of cyclone and a convergent motion there (Fig. 4.5a). There are low and high sea level pressure anomalies (Fig. 4.5b) in the Tropical Atlantic and Pacific, respectively. These correspond to ascending and descending motions (Fig. 4.5b) at the 500hPa, respectively. The high pressure and descending motion anomalies (Fig.

4.5b) in the Tropical Pacific suppress convective activity and reduce precipitation there (Fig. 4.4a). The sea level pressure anomalies further produce easterly wind stress anomalies (Fig. 4.4b). In general, the coupled model with observed SST prescribed in the Tropical Atlantic reproduces the observed relationship (Fig. 4.3a, b) between atmospheric circulation anomalies and Atlantic zonal mode variability very well in both amplitude and phase.

Forced by the easterly wind stress (Fig. 4.4b) associated with the warm SST anomalies of the Atlantic zonal mode, equatorial Pacific thermocline slope is increased, with shallowing and deepening in the east and west (Fig. 4.4b), respectively. The shallower thermocline (Fig. 4.4b) in the eastern Pacific reduces sea surface temperature there (Fig. 4.4a). In the following autumn and winter (Fig. 4.4b, c), the anomalies in wind stress, thermocline depth and SST are enhanced through Bjerknes positive feedback. In general, the coupled model has revealed the same mechanisms of how Atlantic zonal mode influences ENSO as found in observations and reanalysis. In contrast to analysis of observations, where causality can not be determined and results may simply arise by chance, the ensemble mean of five model runs strongly indicates the existence of a physically robust influence of the Atlantic Zonal mode on Pacific interannual variability.

4.5 Conclusion and discussion

In this study we investigate the mechanisms of how the Atlantic zonal mode in boreal summer affects ENSO during boreal winter in the period since 1970. Observations show that the warm (cold) phase of the Atlantic zonal mode during boreal summer favours the development of La Niña (El Niño) during boreal winter. Warm SST anomalies of Atlantic zonal mode are associated with positive precipitation anomalies and more latent heat release, which affects the Walker Circulation. This produces anomalous high sea level pressure and descending motion over the Tropical

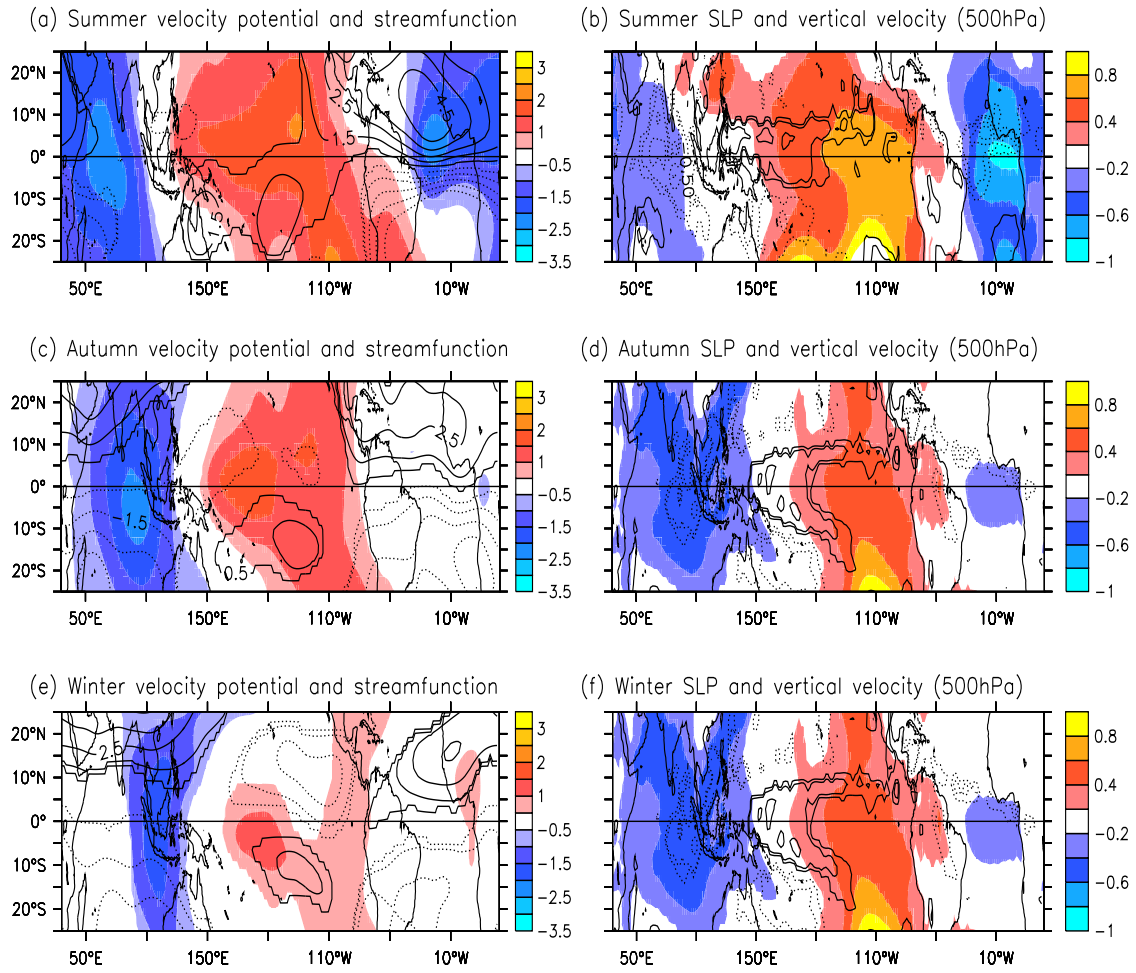

Figure 4.5: (a, c and e) Streamfunction (contour) and velocity potential (shading) and (b, d and f) sea level pressure (shading) and vertical velocity (contour) at the 500hPa in boreal summer (a, b), autumn (c, d) and winter (e, f) regressed onto boreal summer Atlantic cold tongue SST. All of the quantities are from ensemble mean of five model runs. The shading and contours are the same as in Fig. 4.3. Only those values which are over 95% statistically significant under a Student t-test are shown.

Pacific. The anomalous high pressure exerts easterly wind stress anomalies over the western to central equatorial Pacific, which further increases thermocline's east-west slope with shallowing and deepening in the eastern and western Pacific, respectively. The shallower thermocline in the east cools SST there, and cold SST anomalies further produce more eastward wind stress in the west. In the following autumn and

winter, these anomalies in wind stress, thermocline and SST are amplified further by the Bjerknes positive feedback, favouring the development of a La Niña event. The same mechanism works for cold phase of Atlantic zonal mode, but with opposite sign.

This mechanism is supported by simulations with the ECHAM5/MPIOM CGCM for the period 1950-2005. Five ensemble member simulations forced with observed SST in the Tropical Atlantic, but with full air-sea coupling allowed in the Pacific and Indian Oceans, reproduce the observed results very well. This result goes beyond previous studies [*Losada et al.*, 2009; *Rodríguez-Fonseca et al.*, 2009]. In the study by *Losada et al.* [2009] only AGCMs were employed, and thus only the direct atmospheric response could be simulated, but not the subsequent amplification by Bjerknes positive feedback. *Rodríguez-Fonseca et al.* [2009] did employ a coupled model with prescribing SST in the Tropical Atlantic. While their approach is very similar to ours, their model results were not entirely consistent with observations and thus could not support strongly the proposed mechanism. In particular, while the model showed negative SST anomalies in the east Pacific in boreal winter, the amplitude is much weaker than that in observations. More importantly, their model did not show any significant signals associated with Atlantic zonal mode in wind stress, east-west gradient in thermocline depth and SST in the equatorial Pacific in boreal summer. The mechanism revealed by both observations and the coupled model experiments in this study show that these signals in boreal summer, which are seeded by the Atlantic zonal mode, are crucial to the following evolution of ENSO.

To investigate how much SST variability is associated with Atlantic zonal mode, simultaneous correlation (Fig. 4.6a) is calculated between model and observations for all the months from 1970 to 2005. In the eastern equatorial Pacific, the correlation is up to 0.3 and even 0.4 at some points, which indicates about 10% of the SST variability in this region is related to Atlantic zonal mode. In the north-western and

south-western Tropical Pacific and western Tropical Indian, the correlation is also high and up to 0.3 (i.e., also explaining 10% of the SST variability). The monthly stratified correlation between model and observed Niño3 SST (Fig. 4.6b) shows larger values in boreal spring and summer (up to 0.5) than in winter (0.3). This indicates that compared to internal dynamics in the Tropical Pacific, the signal from the Atlantic zonal mode is more important in boreal spring and summer than in winter. Therefore, it is possible for a signal from Atlantic zonal mode to influence the evolution of ENSO at these times. The simultaneous correlation (Fig. 4.6c) is also calculated between model and NCEP reanalysis thermocline depth for all the months. In the equatorial Pacific, the correlation is up to 0.3 in the east and 0.4 in the west, respectively. This shows that about 10%-16% of the thermocline depth variability in the Pacific equatorial belt is associated with the Atlantic zonal mode.

Interestingly, there are also significant influences of the Atlantic zonal mode on the Indian Ocean and the western Pacific. For instance, precipitation anomalies appear in the eastern Indian Ocean and western Pacific in boreal summer. In the following autumn and winter, the anomalies extend northeastward and southeastward, respectively, covering a large part of west Pacific and eastern Indian Ocean. In these regions, there are positive SST anomalies, too. The model also reproduces these precipitation and SST anomalies. However, these relations may not reflect a direct influence of the Atlantic zonal mode [*Kucharski et al.*, 2007], but rather an indirect influence of the induced Pacific variability.

Over the Indian peninsula, neither observation nor our model simulations show significant precipitation anomalies in boreal summer. Anomalies in atmospheric circulation are also not significant during this season. These findings are different from previous studies [*Kucharski et al.*, 2007; 2008; 2009; *Losada et al.*, 2009] that argue that warm SST anomalies in the Tropical Atlantic produce descending motion and reduce rainfall over the Indian peninsula in boreal summer. These studies

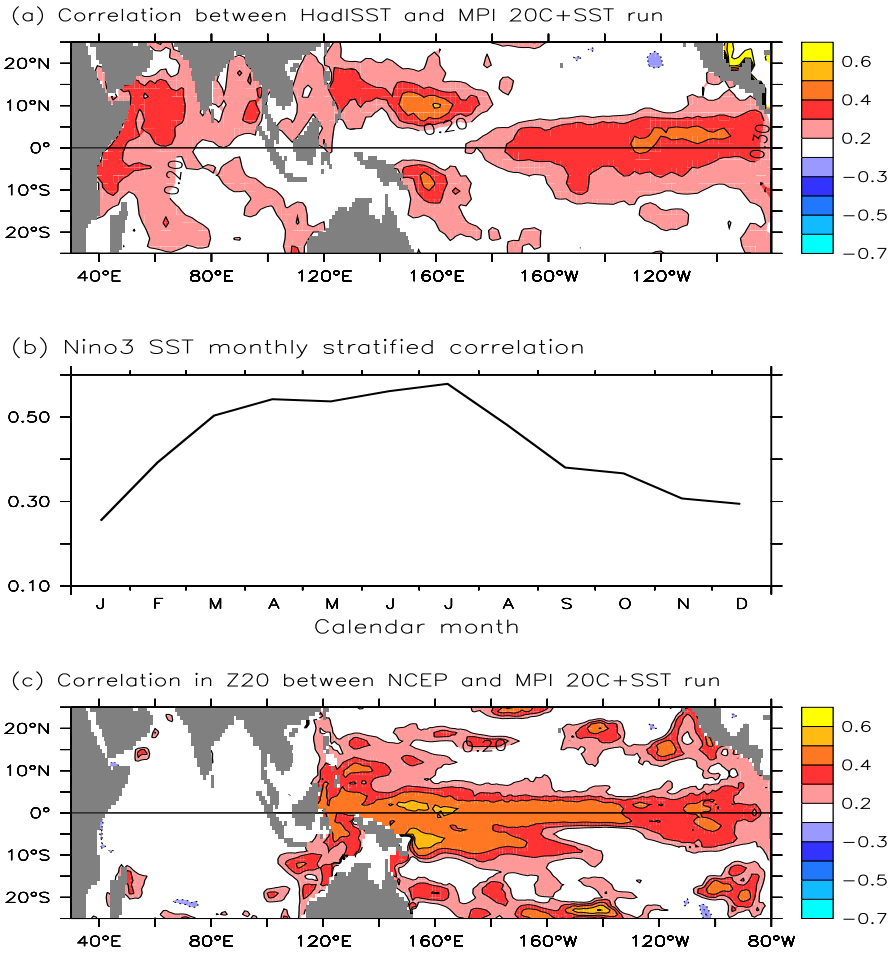

Figure 4.6: (a) Correlation between observed (HadISST) SST and the ensemble mean SST simulated by the MPI model with observed SST prescribed in the Atlantic. (b) As in (a) except for Niño3 SST and for individual calendar months. (c) As in (a) except for thermocline depth between NCEP reanalysis and MPI model.

either employed a regional coupled model for the Indian Ocean [*Kucharski et al.*, 2007; 2008; 2009] or AGCMs [*Losada et al.*, 2009]. In both cases, ocean-atmosphere coupling over the Pacific is excluded. However, previous studies [*Rodríguez-Fonseca et al.*, 2009] and this study indicate that Tropical Pacific variability is not independent of the Atlantic zonal mode. We speculate that direct and indirect influences compete over the Indian peninsula. On one hand, warm SST anomalies in the Tropical Atlantic reduce rainfall there [*Kucharski et al.*, 2007; 2008; 2009; *Losada et al.*,

2009]. On the other hand, the warm SST anomalies produce cold SST anomalies in the eastern Pacific. The cold SST anomalies of ENSO enhance rainfall on the Indian peninsula. These two mechanisms compete and result in an insignificant linear relationship in both observations and the model.

In this study, observed SST from Tropical Atlantic is used to drive the coupled model. However, part of the SST variability in the Tropical Atlantic possibly comes from ENSO's influence with a lag of several months according to numerous previous studies [e.g., *Enfield and Mayer*, 1997; *Carton and Huang*, 1994; *Latif and Barnett*, 1995; *Latif and Grötzner*, 2000; *Chiang and Sobel*, 2002; *Chiang and Lintner*, 2005; *Chang et al.*, 2006]. Our results do not contradict these, but in this case the results should be considered as feedback on ENSO. However, it would imply that variability in the Atlantic may not be useful in increasing ENSO prediction skill, but this deserves further investigation.

Acknowledgments

The work was supported by the German BMBF NORDATLANTIK project and the SFB 754 of DFG. NSK is funded by the DFG Emmy Noether Programme. The coupled model was run in ECMWF. Figures were created using Ferret, a product of NOAA's Pacific Marine Environmental Laboratory.

Chapter 5

Summary

5.1 Main achievements

In this work, I addressed the mechanisms for Tropical Atlantic variability on annual to interannual time scales and for the influence of the Tropical Atlantic on the other tropical oceans. There were three main achievements:

1. **A better understanding of the dynamics of the seasonal cycle of thermocline depth, sea level and surface zonal currents in the equatorial Atlantic.**

    - Linear dynamics can explain the seasonal variation of sea level. They can also explain key features of surface zonal current variations, but variations are far too strong. Nonlinear dynamics are required to weaken the variability to observed levels, and improve its phase and zonal extent.
    - The linear solution is essentially reproduced by the first four baroclinic modes, the Kelvin and first meridional mode Rossby waves, with boundary reflected waves contributing as strongly as directly forced waves.
    - The semi-annual cycle in zonal winds although much weaker than the

annual component forces a strong semi-annual component in sea level and surface zonal currents, because it excites the basin mode of the second baroclinc mode. This explains the observed feature in the seasonal cycle from March to August.

2. An improved understanding of the Atlantic zonal mode, and the role of equatorial heat content.

- The Atlantic zonal mode is an oscillatory normal-mode of the observed coupled system, obeying the delayed-action/recharge oscillator paradigm for ENSO.
- The zonal mode explains a large amount (70%) of SST variability in the east and a significant fraction (19%) of equatorial variability. Thus, the predictability potential in the Equatorial Atlantic on seasonal time scales may be considerably higher than currently thought.

3. Demonstrated a mechanism for the influence of the Atlantic zonal mode on ENSO for the first time using a coupled climate model.

- A warm phase of Atlantic zonal mode during boreal summer favours the development of a La Niña event during the boreal winter and vice versa. SST anomalies associated with Atlantic zonal mode influence the Bjerknes positive feedback loop in the Tropical Pacific, through affecting the Walker Circulation and so wind stress during boreal summer. These signals associated with Atlantic zonal mode are amplified in the following autumn and winter and impact the evolution of ENSO.

5.2 Outlooks

In this section I discuss aspects related to this work that were not addressed and remain poorly understood, but which I believe are worthy of further investigation.

1. **Ocean-atmosphere coupling mechanisms in the equatorial Atlantic annual cycle of sea surface temperature:**

   The annual cycle dominates SST variability in the Tropical Atlantic. It arises from African Monsoon forcing and ocean-atmosphere interaction. However, this ocean-atmosphere interaction is not well understood yet. Previous studies suggested the annual cycle of SST at the equatorial Atlantic stems from coupling mechanisms of mixed layer mode without involving thermocline variations [e.g., *Chang and Philander*, 1994; *Xie*, 1994]. However, in contrast to the Pacific, thermocline depth displays pronounced seasonal variations in the tropical Atlantic. Preliminary analysis (not shown) shows that the seasonal relationship among SST, thermocline depth, and surface zonal currents in the Atlantic appear more consistent with a thermocline mode. Understanding the coupling mechanisms of SST annual cycle is also important for improving coupled climate models [*Stockdale et al.*, 2006; *Richter and Xie*, 2008; *Wahl et al.*, 2009]. *Stockdale et al.* [2006] showed that state-of-the-art coupled climate model cannot correctly simulate the SST annual cycle in the tropical Atlantic, limiting seasonal forecast skills there. The ocean-atmosphere interaction can also amplify model errors in rainfall and surface wind stress in boreal spring [*Richter and Xie*, 2008; *Wahl et al.*, 2009], giving rise to a large warm bias in the eastern tropical Atlantic. This warm bias is one of the key problems in almost all state-of-the-art coupled climate models [*Davey et al.*, 2002; *Richter and Xie*, 2008; *Wahl et al.*, 2009]. Therefore, understanding the ocean-atmosphere coupling mechanisms, which give rise to annual cycle in

SST, should be one of the major tasks in studying Tropical Atlantic variability in the future.

2. Interaction between seasonal cycle and interannual variability:

Different seasonal cycles in ocean dynamics in the Tropical Pacific and Atlantic imply that interaction between seasonal cycle and interannual variability should be different in these two basins. Actually, interannual variability in tropical Pacific and Atlantic has different seasonality [*Philander*, 1990; *Keenlyside and Latif*, 2007; *Okumura and Xie*, 2006]. In the Pacific, ENSO often peaks in boreal winter; while in the Atlantic, zonal mode has major peak in boreal summer and secondary peak in November-December [*Philander*, 1990; *Keenlyside and Latif*, 2007; *Okumura and Xie*, 2006]. Previous studies suggested seasonality of Atlantic zonal mode is coincident with seasonal cycle of thermocline depth [*Keenlyside and Latif*, 2007; *Okumura and Xie*, 2006]. Therefore, interaction between seasonal cycle and interannual variability is another topic worth further investigation. In particular, peaks in the annual cycle and interannual variations in SST occur simultaneously in boreal summer.

3. Other possible mechanisms responsible for interannual variability:

This work showed that the delayed action oscillator/recharge oscillator mechanism dominates in the Atlantic zonal mode. However, the correlation is not high (about 0.4) when equatorial Atlantic heat content leads SST averaged over cold tongue by a few months. One possibility is data quality issues. Alternatively, the recharge oscillator mechanisms may explain much less variance than suggested in our analysis or other dynamics may better describe equatorial Atlantic variability. Other possible mechanisms include, the western Pacific oscillator [*Weisberg and Wang*, 1997], advective-reflective oscilla-

tor [*Picaut et al.*, 1997; *Wang*, 2001], or a destabilized basin mode [*Jin and Neelin*, 1993; *Keenlyside et al.*, 2007]. The western Pacific oscillator, however, is probably not active in the Atlantic, as no negative SST or westward wind stress anomalies exist in the western Atlantic during the zonal mode's peak phase (Fig 3.1b). Zonal current variations are important in both the advective-reflective oscillator and destabilized basin-mode mechanisms. Preliminary analysis of zonal currents, model and satellite-derived, suggest a possible role for the basin mode (not shown). However, explained variances are substantially smaller than that for heat content (SSH and thermocline depth). Further analysis and better ocean heat content data are required to resolve these issues.

Bibliography

Adamec, D., and J. O'Brien (1978), The Seasonal Upwelling in the Gulf of Guinea Due to Remote Forcing, *J. Phys. Oceanogr.*, *8*(6), 1050–1060, doi:10.1175/1520-0485(1978)008<1050:TSUITG>2.0.CO;2.

Antonov, J., R. Locarnini, T. Boyer, A. Mishonov, H. Garcia, and S. Levitus (2006), World Ocean Atlas 2005 Volume 2: Salinity.

Arnault, S., B. Bourlès, Y. Gouriou, and R. Chuchla (1999), Intercomparison of the upper layer circulation of the western equatorial Atlantic Ocean: In situ and satellite data, *J. Geophys. Res.*, *104*(C9), 21,171–21,194, doi:10.1029/1999JC900124.

Bjerknes, J. (1969), Atmospheric Teleconnections from the Equatorial PACIFIC1, *Mon. Wea. Rev.*, *97*(3), 163, doi:10.1175/1520-0493(1969)097<0163:ATFTEP>2.3.CO;2.

Bonjean, F., and G. Lagerloef (2002), Diagnostic Model and Analysis of the Surface Currents in the Tropical Pacific Ocean, *J. Phys. Oceanogr.*, *32*(10), 2938–2954, doi:10.1175/1520-0485(2002)032<2938:DMAAOT>2.0.CO;2.

Brandt, P., and C. Eden (2005), Annual cycle and interannual variability of the mid-depth tropical Atlantic Ocean, *Deep-Sea Res. Part I*, *52*(2), 199–219, doi:10.1016/j.dsr.2004.03.011.

Bunge, L., and A. Clarke (2009), Seasonal propagation of sea level along the equator in the Atlantic, *J. Phys. Oceanogr.*, *39*(4), 10691074, doi:10.1175/2008JPO4003.1.

Burgers, G., F. Jin, and G. Van Oldenborgh (2005), The simplest ENSO recharge oscillator, *Geophys. Res. Lett.*, *32*(13), L13,706, doi:10.1029/2005GL022951.

Busalacchi, A., and J. Picaut (1983), Seasonal Variability from a Model of the Tropical Atlantic Ocean, *J. Phys. Oceanogr.*, *13*(9), 1564–1588, doi:10.1175/1520-0485(1983)013<1564:SVFAMO>2.0.CO;2.

Cane, M., and D. Moore (1981), A Note on Low-Frequency Equatorial Basin Modes, *J. Phys. Oceanogr.*, *11*(11), 1578–1584, doi:10.1175/1520-0485(1981)011<1578:ANOLFE>2.0.CO;2.

Cane, M., and E. Sarachik (1981), The response of a linear baroclinic equatorial ocean to periodic forcing, *J. Mar. Res.*, *39*, 651–693.

Carton, J., and B. Huang (1994), Warm Events in the Tropical Atlantic, *J. Phys. Oceanogr.*, *24*(5), 888–903, doi:10.1175/1520-0485(1994)024<0888:WEITTA>2.0.CO;2.

Carton, J., X. Cao, B. Giese, and A. Da Silva (1996), Decadal and interannual SST variability in the tropical Atlantic Ocean, *J. Phys. Oceanogr.*, *26*(7), 1165–1175, doi:10.1175/1520-0485(1996)026<1165:DAISVI>2.0.CO;2.

Chang, P., and S. G. Philander (1994), A coupled ocean-atmosphere instability of relevance to the seasonal cycle, *J. Atmos. Sci.*, *51*(24), 3627–3648, doi:10.1175/1520-0469(1994)051<3627:ACOIOR>2.0.CO;2.

Chang, P., L. Ji, B. Wang, and T. Li (1995), Interactions between the seasonal cycle and el niño-southern oscillation in an intermediate coupled ocean-atmosphere model, *J. Atmos. Sci.*, *52*(13), 2353–2372, doi:10.1175/1520-0469(1995)052<2353:IBTSCA>2.0.CO;2.

Chang, P., Y. Fang, R. Saravanan, L. Ji, and H. Seidel (2006), The cause of the fragile relationship between the Pacific El Niño and the Atlantic Niño., *Nature*, *443*(7109), 324, doi:10.1038/nature05053.

Chiang, J., and B. Lintner (2005), Mechanisms of remote tropical surface warming during El Niño, *J. Climate*, *18*(20), 4130–4149, doi:10.1175/JCLI3529.1.

Chiang, J., and A. Sobel (2002), Tropical tropospheric temperature variations caused by ENSO and their influence on the remote tropical climate, *J. Climate*, *15*(18), 18, doi:10.1175/1520-0442(2002)015<2616:TTTVCB>2.0.CO;2.

Davey, M., M. Huddleston, K. Sperber, P. Braconnot, F. Bryan, D. Chen, R. Colman, C. Cooper, U. Cubasch, P. Delecluse, et al. (2002), STOIC: a study of coupled model climatology and variability in tropical ocean regions, *Climate Dyn.*, *18*(5), 403–420, doi:10.1007/s00382-001-0188-6.

Ding, H., N. Keenlyside, and M. Latif (2009), Seasonal cycle in the upper equatorial Atlantic Ocean, *J. Geophys. Res.*, *114*(C9), C09,016, doi:10.1029/2009JC005418.

Ding, H., N. Keenlyside, and M. Latif (2010), Equatorial Atlantic interannual variability: the role of heat content, *J. Geophys. Res.*, doi:10.1029/2010JC006304, in press.

du Penhoat, Y., and Y. Gouriou (1987), Hindcasts of equatorial sea surface dynamic height in the Atlantic in 1982-1984, *J. Geophys. Res.*, *92*, 3729–3740.

du Penhoat, Y., and A. Treguier (1985), The seasonal linear response of the tropical Atlantic ocean, *J. Phys. Oceanogr.*, *15*(3), 316–329, doi:10.1175/1520-0485(1985)015.

Enfield, D., and D. Mayer (1997), Tropical Atlantic sea surface temperature variability and its relation to El Nino-Southern Oscillation, *J. Geophys. Res.*, *102*(C1), 929–945, doi:10.1029/96JC03296.

Foltz, G., S. Grodsky, J. Carton, and M. McPhaden (2003), Seasonal mixed layer heat budget of the tropical Atlantic Ocean, *J. Geophys. Res.*, *108*(10.1029), 3146, doi:10.1029/2002JC001584.

Frankignoul, C., and E. Kestenare (2005), Air-sea interactions in the tropical Atlantic: a view based on lagged rotated maximum covariance analysis, *J. Climate*, *18*(18), 3874–3890, doi:10.1175/JCLI3498.1.

Gent, P., K. O'Neill, and M. Cane (1983), A Model of the Semiannual Oscillation in the Equatorial Indian Ocean, *J. Phys. Oceanogr.*, *13*(12), 2148–2160, doi:10.1175/1520-0485(1983)013<2148:AMOTSO>2.0.CO;2.

Gill, A. (1982), Atmosphere-Ocean Dynamics, *International Geophysics Series*, *30*, 662.

Gill, A., and A. Clarke (1974), Wind-induced upwelling, coastal currents and sea-level changes, *Deep-Sea Res*, *21*, 325–345.

Glantz, M., R. Katz, and N. Nicholls (1991), *Teleconnections linking worldwide climate anomalies*, Cambridge University Press Cambridge.

Hasselmann, K. (1988), PIPs and POPs: The Reduction of Complex Dynamical Systems Using Principal Interaction and Oscillation Patterns, *J. Geophys. Res.*, *93*(D9), 11,015–11,021, doi:10.1029/JD093iD09p11015.

Houghton, R. (1983), Seasonal Variations of the Subsurface Thermal Structure in the Gulf of Guinea, *J. Phys. Oceanogr.*, *13*(11), 2070–2081, doi:10.1175/1520-0485(1983)013<2070:SVOTST>2.0.CO;2.

Hu, Z., and B. Huang (2006), Physical processes associated with the tropical Atlantic SST meridional gradient, *J. Climate*, *19*(21), 5500–5518, doi:10.1175/JCLI3923.1.

Hu, Z., and B. Huang (2007), Physical processes associated with the tropical Atlantic SST gradient during the anomalous evolution in the southeastern ocean, *J. Climate*, *20*(14), 3366–3378, doi:10.1175/JCLI4189.1.

Illig, S., and B. Dewitte (2006), Local coupled equatorial variability versus remote ENSO forcing in an intermediate coupled model of the tropical Atlantic, *J. Climate*, *19*(20), 5227–5252, doi:10.1175/JCLI3922.1.

Illig, S., B. Dewitte, N. Ayoub, Y. du Penhoat, G. Reverdin, P. De Mey, F. Bonjean, and G. Lagerloef (2004), Interannual long equatorial waves in the tropical Atlantic from a high-resolution ocean general circulation model experiment in 1981–2000, *J. Geophys. Res.*, *109*(C2), C02,022, doi:10.1029/2003JC001771.

Jansen, M., D. Dommenget, and N. Keenlyside (2009), Tropical atmosphere–ocean interactions in a conceptual framework, *Journal of Climate*, *22*(3), 550–567, doi:10.1175/2008JCLI2243.1.

Jin, F. (1997), An Equatorial Ocean Recharge Paradigm for ENSO. Part I: Conceptual Model, *J. Atmos. Sci.*, *54*(7), 811–829, doi:10.1175/1520-0469(1997)054<0811:AEORPF>2.0.CO;2.

Jin, F., and J. Neelin (1993), Modes of interannual tropical ocean-atmosphere interaction-a unified view. Part I: Numerical results, *J. Atmos. Sci.*, *50*(21), 3477–3477, doi:10.1175/1520-0469(1993)050<3477:MOITOI>2.0.CO;2.

Jungclaus, J., N. Keenlyside, M. Botzet, H. Haak, J. Luo, M. Latif, J. Marotzke, U. Mikolajewicz, and E. Roeckner (2006), Ocean circulation and tropical variability in the coupled model ECHAM5/MPI-OM, *J. Climate*, *19*(16), 3952–3972, doi:10.1175/JCLI3827.1.

Kalnay, E., M. Kanamitsu, R. Kistler, W. Collins, D. Deaven, L. Gandin, M. Iredell, S. Saha, G. White, J. Woollen, et al. (1996), The NCEP/NCAR 40-Year Reanalysis Project, *Bull. Am. Meteorol. Soc.*, *77*(3), 437–471, doi:10.1175/1520-0477(1996)077<0437:TNYRP>2.0.CO;2.

Keenlyside, N., and R. Kleeman (2002), Annual cycle of equatorial zonal currents in the Pacific, *J. Geophys. Res.*, *107*(C8), 3093, doi:10.1029/2000JC000711.

Keenlyside, N., and M. Latif (2007), Understanding Equatorial Atlantic Interannual Variability, *J. Climate*, *20*(1), 131–142, doi:10.1175/JCLI3992.1.

Keenlyside, N., M. Latif, and A. Durkop (2007), On Sub-ENSO Variability, *J. Climate*, *20*(14), 3452–3469, doi:10.1175/JCLI4199.1.

Keenlyside, N., M. Latif, J. Jungclaus, L. Kornblueh, and E. Roeckner (2008), Advancing decadal-scale climate prediction in the North Atlantic sector, *Nature*, *453*(7191), 84–88, doi:10.1038/nature06921.

Keenlyside, N. S. (2001), Improved modeling of zonal currents and SST in the tropical Pacific, Ph.D. thesis, Monash University, Australia.

Kleeman, R., and A. Moore (1999), A new method for determining the reliability of dynamical ENSO predictions, *Mon. Wea. Rev.*, *127*(5), 694–705, doi:10.1175/1520-0493(1999)127<0694:ANMFDT>2.0.CO;2.

Klein, S., B. Soden, and N. Lau (1999), Remote sea surface temperature variations during ENSO: Evidence for a tropical atmospheric bridge, *J. Climate*, *12*(4), 917–932, doi:10.1175/1520-0442(1999)012¡0917:RSSTVD¿2.0.CO;2.

Kozlenko, S., I. Mokhov, and D. Smirnov (2009), Analysis of the cause and effect relationships between El Niño in the Pacific and its analog in the equatorial Atlantic, *Izvestiya Atmospheric and Oceanic Physics*, *45*(6), 704–713, doi:10.1134/S0001433809060036.

Krishnamurthy, V., and B. Kirtman (2006), Variability of the Indian Ocean: Relation to monsoon and ENSO, *Quart. J. Roy. Meteor. Soc.*, *129*(590), 1623–1646, doi:10.1256/qj.01.166.

Kucharski, F., A. Bracco, J. Yoo, and F. Molteni (2007), Low-Frequency Variability of the Indian Monsoon-ENSO Relationship and the Tropical Atlantic: The" Weakening" of the 1980s and 1990s, *J. Climate*, *20*(16), 4255, doi:10.1175/JCLI4254.1.

Kucharski, F., A. Bracco, J. Yoo, and F. Molteni (2008), Atlantic forced component of the Indian monsoon interannual variability, *Geophys. Res. Lett.*, *33*(4), L04,706, doi:10.1029/2007GL033037.

Kucharski, F., A. Bracco, J. Yoo, A. Tompkins, L. Feudale, P. Ruti, and A. Dell'Aquila (2009), A Gill-Matsuno-type mechanism explains the tropical Atlantic influence on African and Indian monsoon rainfall, *Quart. J. Roy. Meteor. Soc*, *135*(640), 569–579, doi:10.1002/qj.406.

Latif, M., and T. Barnett (1995), Interactions of the tropical oceans, *J. Climate*, *8*(4), 952–965, doi:10.1175/1520-0442(1995)008<0952:IOTTO>2.0.CO;2.

Latif, M., and A. Grötzner (2000), The equatorial Atlantic oscillation and its response to ENSO, *Climate Dyn.*, *16*(2), 213–218, doi:10.1007/s003820050014.

Levitus, S., and T. Boyer (1994), World Ocean Atlas, *Washington DC: NOAA*, *1*, 117.

Liu, Z. (2002), A simple model study of enso suppression by external periodic forcing, *J. Climate*, *15*(9), 1088–1098, doi:10.1175/1520-0442(2002)015<1088:ASMSOE>2.0.CO;2.

Locarnini, R., A. Mishonov, J. Antonov, T. Boyer, and H. Garcia (2006), World Ocean Atlas 2005, Vol. 1: Temperature.

Losada, T., B. Rodríguez-Fonseca, I. Polo, S. Janicot, S. Gervois, F. Chauvin, and P. Ruti (2009), Tropical response to the Atlantic Equatorial mode: AGCM multimodel approach, *Climate Dyn.*, *33*(1), 1–8, doi:10.1007/s00382-009-0624-6.

Lübbecke, J., C. Böning, N. Keenlyside, and S.-P. Xie (accepted), On the connection between Benguela and Equatorial Atlantic Niños and the role of the South Atlantic Anticyclone.

Lumpkin, R., and Z. Garraffo (2005), Evaluating the Decomposition of Tropical Atlantic Drifter Observations, *J. Atmos. Oceanic. Technol.*, *22*(9), 1403–1415, doi:10.1175/JTECH1793.1.

Marsland, S., H. Haak, J. Jungclaus, M. Latif, and F. Roske (2003), The Max-Planck-Institute global ocean/sea ice model with orthogonal curvilinear coordinates, *Ocean Model.*, *5*(2), 91–127, doi:10.1016/S1463-5003(02)00015-X.

McCreary, J. (1981), A Linear Stratified Ocean Model of the Coastal Undercurrent, *Philosophical Transactions of the Royal Society of London. Series A, Mathematical and Physical Sciences (1934-1990)*, *302*(1469), 385–413, doi:10.1098/rsta.1981.0176.

McPhaden, M., A. Busalacchi, R. Cheney, J. Donguy, K. Gage, D. Halpern, M. Ji, P. Julian, G. Meyers, G. Mitchum, et al. (1998), The Tropical Ocean-Global Atmosphere observing system: A decade of progress, *J. Geophys. Res.*, *103*, 14,169–14,240.

Meinen, C., and M. McPhaden (2000), Observations of warm water volume changes in the equatorial Pacific and their relationship to El Niño and La Niña, *Journal of Climate*, *13*(20), 3551–3559, doi:10.1175/1520-0442(2000)013<3551:OOWWVC>2.0.CO;2.

Mitchell, T., and J. Wallace (1992), The annual cycle in equatorial convection and sea surface temperature, *J. Climate*, *5*(10), 1140–1156, doi:10.1175/1520-0442(1992)005<1140:TACIEC>2.0.CO;2.

Molinari, R. (1983), Observations of near-surface currents and temperature in the central and western tropical Atlantic ocean, *J. Geophys. Res.*, *88*, 4433–4438.

Okumura, Y., and S. Xie (2006), Some Overlooked Features of Tropical Atlantic Climate Leading to a New Niño-Like Phenomenon*, *J. Climate*, *19*(22), doi:10.1175/JCLI3928.1.

Penland, C., and P. D. Sardeshmukh (1995), The optimal growth of tropical sea surface temperature anomalies, *J. Climate*, *8*(8), 1999–2024, doi:10.1175/1520-0442(1995)008¡1999:TOGOTS¿2.0.CO;2.

Philander, S. (1990), *El Niño, La Niña, and the southern oscillation*, Academic Pr.

Philander, S., and R. Pacanowski (1980), The generation of equatorial currents, *J. Geophys. Res.*, *85*, 1123–1136.

Philander, S., and R. Pacanowski (1986), A model of the seasonal cycle in the tropical Atlantic Ocean, *J. Geophys. Res.*, *91*, 14,192–14,206.

Picaut, J. (1983), Propagation of the Seasonal Upwelling in the Eastern Equatorial Atlantic, *J. Phys. Oceanogr.*, *13*(1), 18–37, doi:10.1175/1520-0485(1983)013<0018:POTSUI>2.0.CO;2.

Picaut, J., F. Masia, and Y. Du Penhoat (1997), An advective-reflective conceptual model for the oscillatory nature of the ENSO, *Science*, *277*(5326), 663, doi:10.1126/science.277.5326.663.

Rayner, N., D. Parker, E. Horton, C. Folland, L. Alexander, D. Rowell, E. Kent, and A. Kaplan (2003), Global analyses of sea surface temperature, sea ice, and night marine air temperature since the late nineteenth century, *J. Geophys. Res.*, *108*(D14), 4407–4453, doi:10.1029/2002JD002670.

Reverdin, G., and M. McPhaden (1986), Near-surface current and temperature variability observed in the equatorial atlantic from drifting buoys, *J. Geophys. Res.*, *91*, 6569–6581.

Reynolds, R. (1988), A Real-Time Global Sea Surface Temperature Analysis, *J. Climate*, *1*(1), 75–87, doi:10.1175/1520-0442(1988)001<0075:ARTGSS>2.0.CO;2.

Reynolds, R., and D. Marsico (1993), An Improved Real-Time Global Sea Surface Temperature Analysis, *J. Climate*, *6*(1), 114–119, doi:10.1175/1520-0442(1993)006<0114:AIRTGS>2.0.CO;2.

Reynolds, R., N. Rayner, T. Smith, D. Stokes, and W. Wang (2002), An Improved In Situ and Satellite SST Analysis for Climate, *J. Climate*, *15*(13), 1609–1625, doi:10.1175/1520-0442(2002)015<1609:AIISAS>2.0.CO;2.

Richardson, P., and T. McKee (1984), Average Seasonal Variation of the Atlantic Equatorial Currents from Historical Ship Drifts, *J. Phys. Oceanogr.*, *14*(7), 1226–1238, doi:10.1175/1520-0485(1984)014<1226:ASVOTA>2.0.CO;2.

Richardson, P., and G. Reverdin (1987), Seasonal cycle of velocity in the Atlantic North Equatorial Countercurrent as measured by surface drifters, current meters, and ship drifts, *J. Geophys. Res.*, *92*, 3691–3708.

Richardson, P., and D. Walsh (1986), Mapping climatological seasonal variations of surface currents in the tropical Atlantic using ship drifts, *J. Geophys. Res.*, *91*(C9), 10,537–10,550, doi:10.1029/JC091iC09p10537.

Richardson, P., S. Arnault, S. Garzoli, and J. Bruce (1992), Annual cycle of the Atlantic North Equatorial contercurrent, *Deep-Sea Res. Part A. Oceanographic research papers*, *39*(6), 997–1014, doi:10.1016/0198-0149(92)90036-S.

Richter, I., and S. Xie (2008), On the origin of equatorial Atlantic biases in coupled general circulation models, *Climate Dyn.*, *31*(5), 587–598, doi:10.1007/s00382-008-0364-z.

Rodríguez-Fonseca, B., I. Polo, J. García-Serrano, T. Losada, E. Mohino, C. Mechoso, and F. Kucharski (2009), Are Atlantic Niños enhancing Pacific ENSO events in recent decades?, *Geophys. Res. Lett.*, *36*(20), L20,705, doi:10.1029/2009GL040048.

Ruiz-Barradas, A., J. Carton, and S. Nigam (2000), Structure of interannual-to-decadal climate variability in the tropical Atlantic sector, *J. Climate*, *13*(18), 3285–3297, doi:10.1175/1520-0442(2000)013<3285:SOITDC>2.0.CO;2.

Schouten, M., R. Matano, and T. Strub (2005), A description of the seasonal cycle of the equatorial Atlantic from altimeter data, *Deep-Sea Res.*, *52*(3), 477–493, doi:10.1016/j.dsr.2004.10.007.

Servain, J., A. Busalacchi, M. McPhaden, A. Moura, G. Reverdin, M. Vianna, and S. Zebiak (1998), A Pilot Research Moored Array in the Tropical Atlantic (PIRATA), *Bull. Am. Meteorol. Soc.*, *79*(10), 2019–2031, doi:10.1175/1520-0477(1998)079<2019:APRMAI>2.0.CO;2.

Stockdale, T., M. Balmaseda, and A. Vidard (2006), Tropical Atlantic SST Prediction with Coupled Ocean–Atmosphere GCMs, *J. Climate*, *19*(23), 6047–6061, doi:10.1175/JCLI3947.1.

Thierry, V., A. Treguier, and H. Mercier (2004), Numerical study of the annual and semi-annual fluctuations in the deep equatorial Atlantic Ocean, *Ocean Model.*, *6*(1), 1–30, doi:10.1016/S1463-5003(02)00054-9.

Tziperman, E., L. Stone, M. Cane, and H. Jarosh (1994), El nino chaos: Overlapping of resonances between the seasonal cycle and the pacific ocean-atmosphere oscillator., *Science*, *264*(5155), 72–74, doi:10.1126/science.264.5155.72.

Valcke, S., A. Caubel, D. Declat, and L. Terray (2003), OASIS3 ocean atmosphere sea ice soil, *Users guide. Prisim project report*, *2*.

von Schuckmann, K., P. Brandt, and C. Eden (2008), Generation of Tropical Instability Waves in the Atlantic Ocean, *J. Geophys. Res.*, *113*(C08034), C08,034, doi:10.1029/2007JC004712.

Von Storch, H., T. Bruns, I. Fischer-Bruns, and K. Hasselmann (1988), Principal Oscillation Pattern Analysis of the 30-to 60-Day Oscillation in General Circulation Model Equatorial Troposphere, *J. Geophys. Res.*, *93*(D9), 11,022–11,036, doi:10.1029/JD093iD09p11022.

Wagner, R., and A. Da Silva (1994), Surface conditions associated with anomalous rainfall in the Guinea coastal region, *Int. J. Climatol.*, *14*(2), 179–199, doi:10.1002/joc.3370140205.

Wahl, S., M. Latif, W. Park, and N. Keenlyside (2009), On the Tropical Atlantic SST warm bias in the Kiel Climate Model, *Climate Dynamics*, *33*(6), 174, doi:10.1007/s00382-009-0690-9.

Wang, C. (2001), A unified oscillator model for the El Niño–Southern Oscillation, *J. Climate*, *14*(1), 98–115, doi:10.1175/1520-0442(2001)014<0098:AUOMFT>2.0.CO;2.

Wang, C. (2006), An overlooked feature of tropical climate: Inter-Pacific-Atlantic variability, *Geophysical Research Letters*, *33*(12), L12,702, doi:10.1029/2006GL026324.

Wang, C., F. Kucharski, R. Barimalala, and A. Bracco (2009), Teleconnections of the tropical Atlantic to the tropical Indian and Pacific Oceans: A review of recent findings, *Meteorologische Zeitschrift*, *18*(4), 445–454, doi:10.1127/0941-2948/2009/0394.

Wang, F., and P. Chang (2008), A Linear Stability Analysis of Coupled Tropical Atlantic Variability, *J. Climate*, *21*(11), 2421–2436, doi:10.1175/2007JCLI2035.1.

Wang, W., and M. McPhaden (1999), The surface-layer heat balance in the equatorial pacific ocean. part i: Mean seasonal cycle, *J. Phys. Oceanogr.*, *29*(8), 1812–1831, doi:10.1175/1520-0485(1999)029<1812:TSLHBI>2.0.CO;2.

Weisberg, R., and T. Tang (1983), Equatorial ocean response to growing and moving wind systems with application to the Atlantic, *J. Mar. Res.*, *41*, 461–486.

Weisberg, R., and T. Tang (1985), On the response of the equatorial thermocline in the Atlantic Ocean to the seasonally varying trade winds, *J. Geophys. Res.*, *90*(C10), 7117–7128, doi:10.1029/JC090iC04p07117.

Weisberg, R., and T. Tang (1987), Further studies on the response of the equatorial thermocline in the Atlantic Ocean to the seasonally varying trade winds, *J. Geophys. Res.*, *92*(C4), 3709–3727, doi:10.1029/JC092iC04p03709.

Weisberg, R., and T. Tang (1990), A Linear Analysis of Equatorial Atlantic Ocean Thermocline Variability, *J. Phys. Oceanogr.*, *20*(12), 1813–1825, doi:10.1175/1520-0485(1990)020<1813:ALAOEA>2.0.CO;2.

Weisberg, R., and C. Wang (1997), A Western Pacific Oscillator Paradigm for the El Niño-Southern Oscillation, *Geophys. Res. Lett.*, *24*(7), 779–782, doi:10.1029/97GL00688.

Xie, P., and P. Arkin (1997), Global precipitation: A 17-year monthly analysis based on gauge observations, satellite estimates, and numerical model outputs, *Bull. Am. Meteorol. Soc.*, *78*(11), 2539–2558, doi:10.1175/1520-0477(1997)078<2539:GPAYMA>2.0.CO;2.

Xie, S. (1994), On the genesis of the equatorial annual cycle, *Journal of Climate*, *7*(12), 2008–2013, doi:10.1175/1520-0442(1994)007<2008:OTGOTE>2.0.CO;2.

Xie, S., and J. Carton (2004), Tropical Atlantic variability: Patterns, mechanisms, and impacts, *Earth's Climate: The Ocean-Atmosphere Interaction, Geophys. Monogr*, *147*, 121–142.

Xie, S.-P., H. Annamalai, F. A. Schott, and J. P. McCreary (2002), Structure and mechanisms of south indian ocean climate variability*, *Journal of Climate*, *15*(8), 864–878, doi:10.1175/1520-0442(2002)015¡0864:SAMOSI¿2.0.CO;2.

Xu, J., and H. Von Storch (1990), Predicting the State of the Southern Oscillation Using Principal Oscillation Pattern Analysis, *Journal of Climate*, *3*(12), 1316–1329, doi:10.1175/1520-0442(1990)003<1316:PTSOTS>2.0.CO;2.

Yu, L., and R. Weller (2007), Objectively Analyzed air-sea heat Fluxes (OAFlux) for the global oceans, *Bull. Am. Meteorol. Soc.*, *88*, 527–539, doi:10.1175/BAMS-88-4-527.

Yu, X., and M. McPhaden (1999), Seasonal Variability in the Equatorial Pacific, *J. Phys. Oceanogr.*, *29*(5), 925–947, doi:10.1175/1520-0485(1999)029<0925:SVITEP>2.0.CO;2.

Zebiak, S. (1993), Air–Sea Interaction in the Equatorial Atlantic Region, *J. Climate*, *6*(8), 1567–1586, doi:10.1175/1520-0442(1993)006<1567:AIITEA>2.0.CO;2.

Publications

1. **Ding, H.**, N. S. Keenlyside, and M. Latif 2009: Seasonal cycle in the upper equatorial Atlantic Ocean, J. Geophys. Res., 114, C09016, doi:10.1029/2009JC005418

2. **Ding, H.**, N. S. Keenlyside, and M. Latif, 2010: Equatorial Atlantic interannual variability: the role of heat content, J. Geophys. Res. Oce., in press

3. **Ding, H.**, N. S. Keenlyside, and M. Latif, 2010: Equatorial Atlantic Impacts on ENSO, J. Geophys. Res. Oce., to be submitted

Acknowledgments

First of all, I must thank my two supervisors Prof. Dr. Mojib Latif and Dr. Noel Keenlyside for the chance to study and work at IFM-GEOMAR. In particular, I must thank Prof. Dr. Mojib Latif for always taking interest in my study, and ensuring its continued progress; and Dr. Noel Keenlyside for his guidance, his enthusiasm in this work, and for his continued supervision. With their help, I could get used to the research environment so that this work is possible.

I would also like to thank our department secretary Connie Schuster for her help during my staying in Kiel. Especially, she gave me great help in dealing with all of the procedures and difficulties when I came here initially.

I must also thank everybody in our department for their help and friendly working environment. Such a friendly environment give me encouragement to study in a foreign country.

Erklärung

Hiermit erkläre ich, dass ich die vorliegende Dissertation, abgesehen von der Beratung durch meine akademischen Lehrer, selbstständig verfasst habe und keine weiteren Quellen und Hilfsmittel als die hier angegebenen verwendet habe. Diese Arbeit hat weder ganz, noch in Teilen, bereits an anderer Stelle einer Prüfungskommission zur Erlangung des Doktorgrades vorgelegen. Ich erkläre, dass die vorliegende Arbeit gemäß der Grundsätze zur Sicherung guter wissenschaftlicher Praxis der Deutschen Forschungsgemeinschaft erstellt wurde.

Kiel, July 21, 2010

(Hui Ding)